Shakedown analysis of engineering structures under multiple variable mechanical and thermal loads using the stress compensation method

Heng Peng[a], Yinghua Liu[a,*], Haofeng Chen[b] and Jun Shen[a]

[a]*Department of Engineering Mechanics, AML, Tsinghua University, Beijing 100084, People's Republic of China*

[b]Department of Mechanical and Aerospace Engineering, University of Strathclyde, Glasgow G1 1XJ, UK

[*]Corresponding author: yhliu@mail.tsinghua.edu.cn

Abstract

The determination of shakedown load or shakedown domain is an important task in structural design and integrity assessment. In this paper, a novel numerical procedure based on the Stress Compensation Method (SCM) is developed to perform shakedown analysis of engineering structures under multiple variable mechanical and thermal loads. By applying the compensation stress on the yield regions that occur at every load vertex of the prescribed loading domain to adjust the total stress to the yield surface and re-solving the equilibrium equations, the statically admissible residual stress field for static shakedown analysis is constructed. A robust and effective iteration control technique with some convergence parameters is used to check the change of the compensation stress in the inner loop and to update the shakedown load multiplier in the outer loop. For the purpose of general use, the method is implemented into ABAQUS platform. The shakedown problems for the Bree plate, a square plate with a central circular hole and a practical thick vessel with nozzles under some two-dimensional and three-dimensional loading domains are effectively solved and analyzed. Both alternating plasticity mechanism and ratcheting mechanism to determine the shakedown boundary of these structures are revealed. Numerical applications show that the proposed method has good numerical stability, high accuracy and efficiency, and is well suited for shakedown analysis of large-scale practical engineering structures.

Keywords: Plasticity; Shakedown analysis; Stress Compensation Method; Cyclic loading; Multi-dimensional loading domain

1 Introduction

In many practical engineering fields, such as electric power, nuclear energy, aerospace, petrochemical and civil industries, structural components are usually subjected to variable repeated mechanical and thermal loads. On the one hand, for making full use of the load-carrying capability of materials, these structural components are allowed to operate in plasticity state. On the other hand, in order to ensure structures to be safe and serviceable, the applied variable loads cannot be beyond the safety margin, i.e. shakedown domain, so that the structural components cannot fail due to alternating plasticity (low-cycle fatigue) or ratcheting (incremental collapse). Therefore, the shakedown analysis has a wide application prospect because of its important theoretical significance and practical engineering value for strengthening the security of structures and reducing costs. Moreover, the determination of shakedown load or shakedown domain of structures becomes the important task in structural design and integrity assessment.

Many designers hope to determine the shakedown limit by the step-by-step incremental elastic-plastic analysis [1, 2], but for complicated loading history the computation is cumbersome and time-consuming. In addition, the exact loading history is often uncertain in practical situations. The shakedown analysis [3-6] based on the lower bound theorem by Melan [3] and the upper bound theorem by Koiter [4] provides an effective approach to calculating the shakedown limit of structures, where the exact loading history is not concerned but only the bounding box of these loads. Since the two classical shakedown theorems [3, 4] were established, the studies on shakedown analysis have attracted broad attention in structural engineering and academic circles (see Refs. [5-44]), mainly involving the theoretical extensions [5-16] and development of numerical methods [7, 17-44] for shakedown analysis.

The two classical shakedown theorems rest on the assumptions [5] of perfectly plastic material, associated temperature-independent constitutive laws, small displacement, negligible inertia and creeping effects. In some engineering situations, these assumptions may be unrealistic. To extend the theory to make it applied in more practical applications, some researchers [6-16] got rid of some coercive assumptions. The shakedown problems of

non-associated flow rules [6, 7], geometrical nonlinearities [8], dynamic effects [9, 10], damaging inelastic material [11, 13] and nonlinear kinematic hardening material [12-16] have been investigated.

However, although the shakedown theories are proposed and extended, a bigger difficulty in practical engineering applications lies on the numerical method for solving the shakedown problem. Shakedown analysis based on the upper and lower bound theorem is mostly transformed as a mathematical programming problem [7, 17-29], which aims to minimize or maximize a goal function with plenty of independent variables and constraint conditions [17]. As one of pioneers in limit and shakedown analysis field, Maier [6] adapted shakedown theory to the linear programming method using piecewise linearization of yield surfaces. If the von Mises yield criterion is used, the mathematical programming formulation for shakedown analysis leads to a complicated nonlinear optimization problem. Over the last four decades, with the rapid development of numerical methods, some powerful algorithms such as the nonlinear Newton-type iteration algorithm [7, 20-22], the second order cone programming (SQCP) [23, 24] and the interior point method (IPM) [25-29] have been developed to solve the nonlinear optimization problem. Besides, some other computational methods [30-35] of structural analysis instead of traditional finite element method have been combined with shakedown theory to solve the shakedown problem.

Going around the difficulties of optimization, Ponter and Chen [36-39, 45] developed the elastic compensation method (ECM) or the linear matching method (LMM) to solve the shakedown problem. Using more physical arguments, the LMM matches the linear behavior to the nonlinear plastic behavior by performing a sequence of linear solutions with spatially varying moduli [38], and the incompressible and kinematically admissible strain rate history is also constructed at the same time. Then a series of monotonically reducing upper bounds are generated by an iterative scheme making full use of the upper shakedown theorem. More recently, the residual stress decomposition method for shakedown (RSDM-S) [41, 46] was proposed for the shakedown analysis of some simple two-dimensional structures under mechanical and thermal loads.

Using these proposed numerical methods, the shakedown limits or shakedown domains of some structures such as tubes, holed plates, continuous beams, pressure vessels and piping,

are calculated. However, it should be mentioned that most of these applications are restricted to some specific cases (plane problem and axisymmetric shells under two loads) and the computational models are relatively simple. In practical industrial applications, engineering structures are often complex and subjected to multiple variable loads. After mesh discretization, the large number of optimization variables and constraints generally result in a tremendous mathematical programming problem, which implies these methods are of low computational efficiency. Moreover, the computing scale of the mathematical programming problem is multiplied with the increase of the vertices of the loading domain.

The purpose of this paper is to develop a novel and effective numerical procedure based on the Stress Compensation Method (SCM) to solve the practical shakedown problems of large-scale engineering structures under multiple variable mechanical and thermal loads. Differing from the LMM that modifies elastic moduli of the material to match the stress to the yield surface, the SCM directly adjusts the stress to the yield surface by applying the compensation stress on the yield regions. The residual stresses for static shakedown analysis are calculated iteratively at the end of a load cycle instead of at every load vertex, by which the proposed method achieves the good performance that the computational time has little relationship with the number of dimensions of loading domain. Moreover, an iterative procedure rather than mathematical programming formulation is established to generate a sequence of descending load multipliers approaching to the shakedown limit. Over the whole procedure, the global stiffness matrix is decomposed only once, which ensures the high computational efficiency of shakedown analysis regardless of the number of the vertices of the loading domain. Different types of Bree problem with two-dimensional loading domain are tested for the verification purpose of the proposed method. A square plate with a central circular hole considering different load combinations in three-dimensional loading space is calculated and analyzed. Finally, the method is effectively applied for solving the practical shakedown problems of a thick vessel with nozzles from nuclear reactor plant.

2 Basic theory of shakedown analysis

If a structure made up of elastic-perfectly plastic material is subjected to some complex

cyclic history of mechanical and thermal loads, the following situations are possible with the increase of the applied loads [5]:

(1) Elastic behavior: If the loads remain sufficiently low, the structural response is perfectly elastic throughout the cycle.

(2) Shakedown: The plastic deformation occurs in some local parts of the structure during the initial several load cycles. Afterwards, the development of plastic deformation terminates and the body possesses a time-independent residual stress field that keeps the total stress within yield.

(3) Alternating plasticity: The plastic strain increments change sign in every load cycle, but the accumulation of strains over the cycle is equal to zero.

(4) Ratcheting: The plastic strains will accumulate in every load cycle. Moreover, the total strains can become so large after a number of cycles that the structure departs from its original form and loses its serviceability.

(5) Plastic collapse: If the loads become sufficiently high, the body plastically collapses at the first load cycle.

The main purpose of the shakedown analysis is to evaluate the shakedown limits or loading domains of structures under variable repeated loads.

2.1 Static shakedown theorem by Melan

As formulated for a three-dimensional situation by Melan [3] in 1938, the static shakedown theorem can be stated as follows: the structure will shake down to the variable repeated loads, i.e., its behavior after several initial load cycles will become purely elastic, if there exists a time-independent distribution of residual stress field $\boldsymbol{\rho}(\mathbf{x})$ such that its superposition with the fictitious elastic stress field $\boldsymbol{\sigma}^{\mathrm{E}}(\mathbf{x},\mathrm{t})$ multiplying by a multiplier λ, satisfies yield criterion of material at any point of the structure under any combination of loads inside prescribed limit, namely:

$$\boldsymbol{\sigma}(\mathbf{x},\mathrm{t}) = \lambda\boldsymbol{\sigma}^{\mathrm{E}}(\mathbf{x},\mathrm{t}) + \boldsymbol{\rho}(\mathbf{x}) \tag{1}$$

$$\begin{aligned} & f\left(\boldsymbol{\sigma}\left(\mathbf{x},t\right)\right)\le 0 \qquad \forall \mathbf{x}\in\boldsymbol{\Omega},\ \forall t \\ & \nabla\cdot\boldsymbol{\rho}\left(\mathbf{x}\right)=\mathbf{0} \qquad \text{in } \boldsymbol{\Omega} \\ & \boldsymbol{\rho}\left(\mathbf{x}\right)\cdot\mathbf{n}=\mathbf{0} \qquad \text{on } \boldsymbol{\Gamma}_t \end{aligned} \tag{2}$$

Here, $\boldsymbol{\sigma}\left(\mathbf{x},t\right)$ is the total stress field; $f\left(\cdot\right)$ denotes the yield function; λ is the shakedown load multiplier; $\nabla\cdot$ denotes the divergence operator; $\boldsymbol{\rho}\left(\mathbf{x}\right)$ represents a self-equilibrated residual stress field which satisfies the equilibrium conditions within the body $\boldsymbol{\Omega}$ and the boundary conditions on the part $\boldsymbol{\Gamma}_t$ of the surface; and $\mathbf{n}$ is the unit outward normal vector of the boundary $\boldsymbol{\Gamma}_t$.

2.2 Loading domain and shakedown load multiplier

If a structure is subjected to an arbitrary finite number N of loadings $\mathbf{P}_i\left(\mathbf{x},t\right)$. The loading history $\mathbf{P}\left(\mathbf{x},t\right)$ can be described as the combinations of the N loading cases, where each loading case $\mathbf{P}_i\left(\mathbf{x},t\right)$ can be decided by time-dependent multiplier $\mu_i\left(t\right)$ and the constant load system $\mathbf{P}_i^0\left(\mathbf{x}\right)$, that is

$$\mathbf{P}\left(\mathbf{x},t\right)=\sum_{i=1}^{N}\mathbf{P}_i\left(\mathbf{x},t\right)=\sum_{i=1}^{N}\mu_i\left(t\right)\mathbf{P}_i^0\left(\mathbf{x}\right) \tag{3}$$

If the bounding values of each multiplier are given as follows:

$$\mu_i^-\le\mu_i\left(t\right)\le\mu_i^+, \qquad i=1,\cdots,N \tag{4}$$

Eq. (3) will describe a domain $\boldsymbol{\Omega}$ of these loads. The loading domain $\boldsymbol{\Omega}$ is usually a convex hyper-polyhedron defined by the vertices in the space of load parameters.

For an elastic body, the elastic stress field is unique to the applied loads of the structure. Thus, the loading domain $\boldsymbol{\Omega}$ will produce the unique domain **E** of the elastic stress at every point of the body. As shown in Fig. 1, a two-dimensional fictitious elastic domain **E** with four vertices B^1, B^2, B^3, B^4 is taken as an example. If the applied loads (or the structural stresses) vary within the loading domain $\boldsymbol{\Omega}$ (or the fictitious elastic domain **E**), the structural safety with respect to shakedown can be evaluated by a multiplier λ which is called shakedown

load multiplier being used for zooming the loading domain $\boldsymbol{\Omega}$ and allowing for the shakedown of the structure.

2.3 A geometrical interpretation of static shakedown analysis

From the geometrical point of view, the basic ideas of static shakedown analysis can be illustrated in Fig. 1. The elastic domain **E** at every point of a structure should be placed into the geometric space formed by the yield surface $\mathrm{f}(\boldsymbol{\sigma})=0$. However, all these elastic domains **E** can only be adjusted by means of translation and scaling, and the mutual movement among these elastic domains must satisfy certain inherent relations. The corresponding physical interpretation is as follows: the translation of these elastic domains compels the residual stress to be constant over a load cycle; the inherent relations represent the self-equilibrium conditions of the residual stress field of the whole body; and the maximum scaling factor is the shakedown load multiplier. Thus, the most critical task for shakedown analysis is to search the optimum residual stress field.

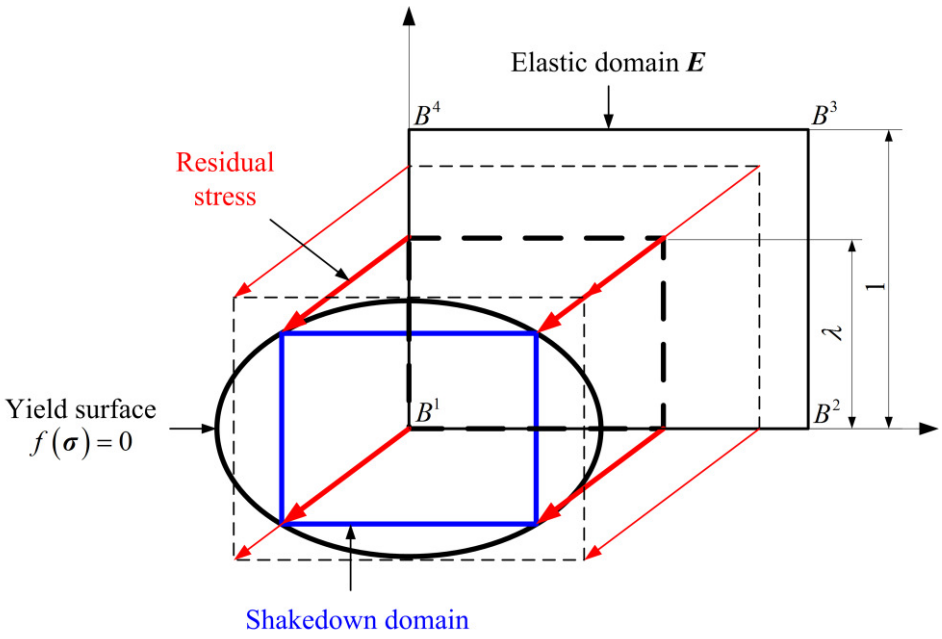

Fig. 1. Illustration of the basic ideas of static shakedown theorem.

3 Novel SCM for mechanical and thermal loads

We suppose that the structure is made up of elastic-perfectly plastic material obeying the

Drucker's postulate. The strain rate $\dot{\boldsymbol{\varepsilon}}(t)$ is decomposed into three parts:

$$\dot{\boldsymbol{\varepsilon}}(t)=\lambda\left[\dot{\boldsymbol{\varepsilon}}^{E}(t)+\dot{\boldsymbol{\varepsilon}}_{\theta}(t)\right]+\dot{\boldsymbol{\varepsilon}}_{r}(t) \tag{5}$$

where $\dot{\boldsymbol{\varepsilon}}^{E}(t)$ is the elastic strain rate corresponding to the fictitious elastic stress rate $\dot{\boldsymbol{\sigma}}^{E}(t)$; $\dot{\boldsymbol{\varepsilon}}_{\theta}(t)$ is the thermal strain rate; and $\dot{\boldsymbol{\varepsilon}}_{r}(t)$ is the residual strain rate. It is worth noting that the residual strain rate $\dot{\boldsymbol{\varepsilon}}_{r}(t)$ consists of the plastic part $\dot{\boldsymbol{\varepsilon}}^{p}(t)$ and the elastic part $\dot{\boldsymbol{\varepsilon}}_{r}^{e}(t)$, and the elastic term $\dot{\boldsymbol{\varepsilon}}_{r}^{e}(t)$ is generated to satisfy the deformation compatibility of the whole body. Then Eq. (5) is written as

$$\dot{\boldsymbol{\varepsilon}}(t)=\lambda\left[\dot{\boldsymbol{\varepsilon}}^{E}(t)+\dot{\boldsymbol{\varepsilon}}_{\theta}(t)\right]+\dot{\boldsymbol{\varepsilon}}^{p}(t)+\dot{\boldsymbol{\varepsilon}}_{r}^{e}(t) \tag{6}$$

According to the constitutive law of elastic-perfectly plastic material with the associated flow rule, the stresses and strains are related by:

$$\dot{\boldsymbol{\sigma}}^{E}(t)=\mathbf{D}\cdot\dot{\boldsymbol{\varepsilon}}^{E}(t) \tag{7}$$

$$\dot{\boldsymbol{\rho}}(t)=\mathbf{D}\cdot\dot{\boldsymbol{\varepsilon}}_{r}^{e}(t) \tag{8}$$

$$\dot{\boldsymbol{\varepsilon}}^{p}(t)=\gamma\frac{\partial f}{\partial\boldsymbol{\sigma}} \tag{9}$$

where $\mathbf{D}$ is the elastic stiffness matrix; f is the yield function; $\dot{\boldsymbol{\varepsilon}}^{p}(t)$ is the plastic strain rate whose direction is along the outer normal of the yield surface; and γ is the plastic multiplier.

For a finite element model, the strains and the stresses are calculated at the Gauss points of the element. The strain rate $\dot{\boldsymbol{\varepsilon}}(t)$ at the Gauss point is related to the nodal displacement rate $\dot{\mathbf{u}}(t)$ of the element:

$$\dot{\boldsymbol{\varepsilon}}(t)=\mathbf{B}\cdot\dot{\mathbf{u}}(t) \tag{10}$$

where $\mathbf{B}$ is the strain-displacement matrix.

Substituting Eq. (6) into (8), the residual stress rate at the Gauss point is written as

$$\dot{\boldsymbol{\rho}}(t)=\mathbf{D}\cdot\left\{\dot{\boldsymbol{\varepsilon}}(t)-\lambda\left[\dot{\boldsymbol{\varepsilon}}^{E}(t)+\dot{\boldsymbol{\varepsilon}}_{\theta}(t)\right]-\dot{\boldsymbol{\varepsilon}}^{p}(t)\right\} \tag{11}$$

Since the residual stress rate field $\dot{\boldsymbol{\rho}}(t)$ is self-equilibrated and the strain rate $\dot{\boldsymbol{\varepsilon}}(t)$ is

kinematically admissible, the principle of virtual work states as follows:

$$\int_V \delta\dot{\boldsymbol{\varepsilon}}^T(t)\cdot\dot{\boldsymbol{\rho}}(t)\mathrm{d}V = 0 \tag{12}$$

where the superscript T denotes the symbol of transpose and $\delta\dot{\boldsymbol{\varepsilon}}(t)$ is the virtual strain rate.

Substituting Eqs. (10) and (11) into Eq. (12), we get

$$\delta\dot{\mathbf{u}}^T(t)\cdot\left\{\int_V \mathbf{B}^T\cdot\mathbf{D}\cdot\left[\mathbf{B}\cdot\dot{\mathbf{u}}(t)-\lambda\left[\dot{\boldsymbol{\varepsilon}}^E(t)+\dot{\boldsymbol{\varepsilon}}_\theta(t)\right]-\dot{\boldsymbol{\varepsilon}}^P(t)\right]\mathrm{d}V\right\}=0 \tag{13}$$

Since Eq. (13) holds for any virtual displacement rate $\delta\dot{\mathbf{u}}(t)$, the integral formula consisting in the equation must vanish, i.e.

$$\left(\int_V \mathbf{B}^T\cdot\mathbf{D}\cdot\mathbf{B}\mathrm{d}V\right)\cdot\dot{\mathbf{u}}(t)=\lambda\int_V \mathbf{B}^T\cdot\mathbf{D}\cdot\left[\dot{\boldsymbol{\varepsilon}}^E(t)+\dot{\boldsymbol{\varepsilon}}_\theta(t)\right]\mathrm{d}V+\int_V \mathbf{B}^T\cdot\mathbf{D}\cdot\dot{\boldsymbol{\varepsilon}}^P(t)\mathrm{d}V \tag{14}$$

We replace the term $\mathbf{D}\cdot\dot{\boldsymbol{\varepsilon}}^P(t)$ with $\boldsymbol{\sigma}^C(t)$ which is named as the compensation stress here, and substitute Eqs. (7) and (10) into Eqs. (14) and (11). Then Eqs. (14) and (11) become, respectively

$$\begin{gathered}\mathbf{K}\cdot\dot{\mathbf{u}}(t)=\lambda\int_V \mathbf{B}^T\cdot\dot{\boldsymbol{\sigma}}^E(t)\mathrm{d}V+\lambda\int_V \mathbf{B}^T\cdot\mathbf{D}\cdot\dot{\boldsymbol{\varepsilon}}_\theta(t)\mathrm{d}V+\int_V \mathbf{B}^T\cdot\boldsymbol{\sigma}^C(t)\mathrm{d}V\\ \mathbf{K}=\int_V \mathbf{B}^T\cdot\mathbf{D}\cdot\mathbf{B}\mathrm{d}V\end{gathered} \tag{15}$$

$$\dot{\boldsymbol{\rho}}(t)=\mathbf{D}\cdot\mathbf{B}\cdot\dot{\mathbf{u}}(t)-\lambda\dot{\boldsymbol{\sigma}}^E(t)-\lambda\mathbf{D}\cdot\dot{\boldsymbol{\varepsilon}}_\theta(t)-\boldsymbol{\sigma}^C(t) \tag{16}$$

where $\mathbf{K}$ is the global stiffness matrix of the structure. Then the residual stress for shakedown analysis is calculated by

$$\boldsymbol{\rho}(t+\Delta t)=\boldsymbol{\rho}(t)+\int_t^{t+\Delta t}\dot{\boldsymbol{\rho}}(t)\mathrm{d}t \tag{17}$$

For load vertex i, the total stresses at all the Gauss points in a body are calculated:

$$\boldsymbol{\sigma}(t_i)=\lambda\boldsymbol{\sigma}^E(t_i)+\boldsymbol{\rho}(t_i) \tag{18}$$

It should be noted that t_i denotes the stress state of the body at the load vertex i. As illustrated in Fig. 2, the total stress vector $\overrightarrow{OC}$ ($\boldsymbol{\sigma}(t_i)$) is equal to the sum of the residual stress vector $\overrightarrow{OD}$ ($\boldsymbol{\rho}(t_i)$) and the fictitious elastic stress vector $\overrightarrow{DC}$ ($\lambda\boldsymbol{\sigma}^E(t_i)$), and the part in excess of the von Mises yield surface is defined as the compensation stress vector $\overrightarrow{AC}$ ($\boldsymbol{\sigma}^C(t_i)$) which is calculated by the following formulae:

$$\boldsymbol{\sigma}^{\mathrm{C}}\left(\mathrm{t}_{\mathrm{i}}\right)=\xi\left(\mathrm{t}_{\mathrm{i}}\right)\cdot\boldsymbol{\sigma}\left(\mathrm{t}_{\mathrm{i}}\right),\quad \xi\left(\mathrm{t}_{\mathrm{i}}\right)=\begin{cases}\dfrac{\bar{\sigma}\left(\mathrm{t}_{\mathrm{i}}\right)-\sigma_{\mathrm{y}}}{\bar{\sigma}\left(\mathrm{t}_{\mathrm{i}}\right)} & \left(\bar{\sigma}\left(\mathrm{t}_{\mathrm{i}}\right)>\sigma_{\mathrm{y}}\right)\\ 0 & \left(\bar{\sigma}\left(\mathrm{t}_{\mathrm{i}}\right)\le\sigma_{\mathrm{y}}\right)\end{cases} \tag{19}$$

If we substitute Eq. (19) into (15), the nodal displacement rate $\dot{\mathbf{u}}\left(\mathrm{t}_{\mathrm{i}}\right)$ can be obtained by solving the equilibrium equations in Eq. (15). Then, a new residual stress field $\boldsymbol{\rho}\left(\mathrm{t}_{\mathrm{i}}\right)$ can be updated by Eq. (17).

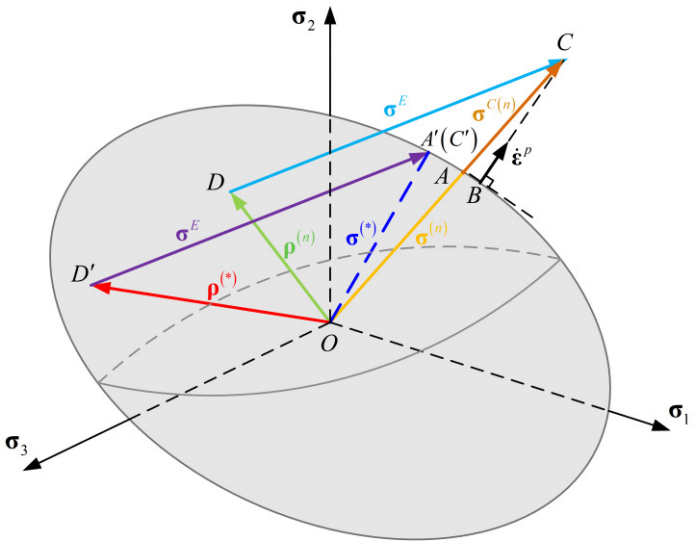

Fig. 2. Von Mises yield surface and stress superposition schematic.

Because the equilibrium equations in Eq. (15) are established for every load vertex, it will require more time to solve these equilibrium equations with the increase of the number of vertices. Now, we superpose all the expressions (Eq. (20)) of residual stress rates over a load cycle.

$$\begin{aligned}\dot{\boldsymbol{\rho}}\left(\mathrm{t}_1\right)&=\mathbf{D}\cdot\mathbf{B}\cdot\dot{\mathbf{u}}\left(\mathrm{t}_1\right)-\lambda\dot{\boldsymbol{\sigma}}^{\mathrm{E}}\left(\mathrm{t}_1\right)-\lambda\mathbf{D}\cdot\dot{\boldsymbol{\varepsilon}}_{\theta}\left(\mathrm{t}_1\right)-\boldsymbol{\sigma}^{\mathrm{C}}\left(\mathrm{t}_1\right)\\ \dot{\boldsymbol{\rho}}\left(\mathrm{t}_2\right)&=\mathbf{D}\cdot\mathbf{B}\cdot\dot{\mathbf{u}}\left(\mathrm{t}_2\right)-\lambda\dot{\boldsymbol{\sigma}}^{\mathrm{E}}\left(\mathrm{t}_2\right)-\lambda\mathbf{D}\cdot\dot{\boldsymbol{\varepsilon}}_{\theta}\left(\mathrm{t}_2\right)-\boldsymbol{\sigma}^{\mathrm{C}}\left(\mathrm{t}_2\right)\\ &\vdots\\ \dot{\boldsymbol{\rho}}\left(\mathrm{t}_{\mathrm{NV}}\right)&=\mathbf{D}\cdot\mathbf{B}\cdot\dot{\mathbf{u}}\left(\mathrm{t}_{\mathrm{NV}}\right)-\lambda\dot{\boldsymbol{\sigma}}^{\mathrm{E}}\left(\mathrm{t}_{\mathrm{NV}}\right)-\lambda\mathbf{D}\cdot\dot{\boldsymbol{\varepsilon}}_{\theta}\left(\mathrm{t}_{\mathrm{NV}}\right)-\boldsymbol{\sigma}^{\mathrm{C}}\left(\mathrm{t}_{\mathrm{NV}}\right)\end{aligned} \tag{20}$$

Then the residual stress rates can be written as

$$\begin{aligned}\dot{\boldsymbol{\rho}}\left(\mathrm{t}^{*}\right)&=\mathbf{D}\cdot\mathbf{B}\cdot\dot{\mathbf{u}}\left(\mathrm{t}^{*}\right)-\lambda\dot{\boldsymbol{\sigma}}^{\mathrm{E}}\left(\mathrm{t}^{*}\right)-\lambda\mathbf{D}\cdot\dot{\boldsymbol{\varepsilon}}_{\theta}\left(\mathrm{t}^{*}\right)-\boldsymbol{\sigma}^{\mathrm{C}}\left(\mathrm{t}^{*}\right)\\ \dot{\boldsymbol{\rho}}_{0}&=\frac{1}{\mathrm{NV}}\dot{\boldsymbol{\rho}}\left(\mathrm{t}^{*}\right)\end{aligned} \tag{21}$$

where

$$
\begin{aligned}
\dot{\boldsymbol{\rho}}\left(\mathrm{t}^{*}\right) &= \dot{\boldsymbol{\rho}}\left(\mathrm{t}_{1}\right)+\dot{\boldsymbol{\rho}}\left(\mathrm{t}_{2}\right)+\cdots+\dot{\boldsymbol{\rho}}\left(\mathrm{t}_{\mathrm{NV}}\right)\\
\dot{\mathbf{u}}\left(\mathrm{t}^{*}\right) &= \dot{\mathbf{u}}\left(\mathrm{t}_{1}\right)+\dot{\mathbf{u}}\left(\mathrm{t}_{2}\right)+\cdots+\dot{\mathbf{u}}\left(\mathrm{t}_{\mathrm{NV}}\right)\\
\dot{\boldsymbol{\sigma}}^{\mathrm{E}}\left(\mathrm{t}^{*}\right) &= \dot{\boldsymbol{\sigma}}^{\mathrm{E}}\left(\mathrm{t}_{1}\right)+\dot{\boldsymbol{\sigma}}^{\mathrm{E}}\left(\mathrm{t}_{2}\right)+\cdots+\dot{\boldsymbol{\sigma}}^{\mathrm{E}}\left(\mathrm{t}_{\mathrm{NV}}\right)\\
\dot{\boldsymbol{\varepsilon}}_{\theta}\left(\mathrm{t}^{*}\right) &= \dot{\boldsymbol{\varepsilon}}_{\theta}\left(\mathrm{t}_{1}\right)+\dot{\boldsymbol{\varepsilon}}_{\theta}\left(\mathrm{t}_{2}\right)+\cdots+\dot{\boldsymbol{\varepsilon}}_{\theta}\left(\mathrm{t}_{\mathrm{NV}}\right)\\
\boldsymbol{\sigma}^{\mathrm{C}}\left(\mathrm{t}^{*}\right) &= \boldsymbol{\sigma}^{\mathrm{C}}\left(\mathrm{t}_{1}\right)+\boldsymbol{\sigma}^{\mathrm{C}}\left(\mathrm{t}_{2}\right)+\cdots+\boldsymbol{\sigma}^{\mathrm{C}}\left(\mathrm{t}_{\mathrm{NV}}\right)
\end{aligned}
\tag{22}
$$

Here, $\dot{\boldsymbol{\rho}}_{0}$ is the updated residual stress rate of the structure for shakedown analysis, and NV denotes the number of vertices within a load cycle. By this way, the equilibrium equations in Eq. (15) just need to be solved only once for every load cycle.

The iterative procedure can be summarized as follows, for the iteration m:

(1) If $\mathrm{m}=1$, the residual stress field $\boldsymbol{\rho}_{0}^{(1)}$ is initialized to zero. Calculate the total stresses $\boldsymbol{\sigma}^{(\mathrm{m})}\left(\mathrm{t}_{\mathrm{i}}\right)$ at all the Gauss points in a body for each load vertex i.

$$
\boldsymbol{\sigma}^{(\mathrm{m})}\left(\mathrm{t}_{\mathrm{i}}\right)=\lambda^{(\mathrm{k})}\boldsymbol{\sigma}^{\mathrm{E}}\left(\mathrm{t}_{\mathrm{i}}\right)+\boldsymbol{\rho}_{0}^{(\mathrm{m})},\qquad \mathrm{i}=1,2,\cdots,\mathrm{NV} \tag{23}
$$

(2) Check whether the total stress $\boldsymbol{\sigma}^{(\mathrm{m})}\left(\mathrm{t}_{\mathrm{i}}\right)$ at every Gauss point of the body exceeds the von Mises yield surface $\mathrm{f}\left(\boldsymbol{\sigma}\right)=0$ for the NV vertices of a load cycle, and calculate the corresponding compensation stress $\boldsymbol{\sigma}^{\mathrm{C}(\mathrm{m})}\left(\mathrm{t}_{\mathrm{i}}\right)$.

(3) Solve the global equilibrium equations in Eq. (24) to obtain the nodal displacement rate $\dot{\mathbf{u}}^{(\mathrm{m+1})}\left(\mathrm{t}^{*}\right)$ for next iteration. Then a new residual stress field $\boldsymbol{\rho}_{0}^{(\mathrm{m+1})}$ can be updated by Eqs. (25)-(27).

$$
\mathbf{K}\cdot\dot{\mathbf{u}}^{(\mathrm{m+1})}\left(\mathrm{t}^{*}\right)=\sum_{\mathrm{i=1}}^{\mathrm{NV}}\left\{\lambda^{(\mathrm{k})}\int_{\mathrm{V}}\mathbf{B}^{\mathrm{T}}\cdot\left[\dot{\boldsymbol{\sigma}}^{\mathrm{E}}\left(\mathrm{t}_{\mathrm{i}}\right)+\mathbf{D}\cdot\dot{\boldsymbol{\varepsilon}}_{\theta}\left(\mathrm{t}_{\mathrm{i}}\right)\right]\mathrm{dV}+\int_{\mathrm{V}}\mathbf{B}^{\mathrm{T}}\cdot\boldsymbol{\sigma}^{\mathrm{C}(\mathrm{m})}\left(\mathrm{t}_{\mathrm{i}}\right)\mathrm{dV}\right\} \tag{24}
$$

$$
\dot{\boldsymbol{\rho}}\left(\mathrm{t}^{*}\right)=\mathbf{D}\cdot\mathbf{B}\cdot\dot{\mathbf{u}}^{(\mathrm{m+1})}\left(\mathrm{t}^{*}\right)-\sum_{\mathrm{i=1}}^{\mathrm{NV}}\left[\lambda^{(\mathrm{k})}\dot{\boldsymbol{\sigma}}^{\mathrm{E}}\left(\mathrm{t}_{\mathrm{i}}\right)+\lambda^{(\mathrm{k})}\mathbf{D}\cdot\dot{\boldsymbol{\varepsilon}}_{\theta}\left(\mathrm{t}_{\mathrm{i}}\right)+\boldsymbol{\sigma}^{\mathrm{C}}\left(\mathrm{t}_{\mathrm{i}}\right)\right] \tag{25}
$$

$$
\dot{\boldsymbol{\rho}}_{0}=\frac{1}{\mathrm{NV}}\dot{\boldsymbol{\rho}}\left(\mathrm{t}^{*}\right) \tag{26}
$$

$$
\boldsymbol{\rho}_{0}^{(\mathrm{m+1})}=\boldsymbol{\rho}_{0}^{(\mathrm{m})}+\int_{\mathrm{t}}^{\mathrm{t+t}^{*}}\dot{\boldsymbol{\rho}}_{0}\mathrm{dt} \tag{27}
$$

(4) Check the change of the value of the compensation stress $\boldsymbol{\sigma}^{\mathrm{C}(\mathrm{m})}\left(\mathrm{t}_{\mathrm{i}}\right)$, and repeat the steps 1-3 till the iterative process converges.

It is worth noting that the convergence of the compensation stress $\boldsymbol{\sigma}^{C(m)}(t_i)$ is equivalent to Condition (28)

$$\left|\xi^{(m+1)}(t_i)-\xi^{(m)}(t_i)\right|\le \mathrm{tol1} \tag{28}$$

where tol1 is a tolerance parameter which dynamically reduces according to the value of $\xi^{(m)}(t_i)$.

The above procedure provides an efficient strategy to search the statically admissible constant residual stress field for shakedown analysis. Each iteration will generate a new self-equilibrated residual stress field. For every vertex of a load cycle, the conditions of the static shakedown theorem are examined. If the conditions of the static shakedown theorem are violated, the compensation stress $\boldsymbol{\sigma}^{C}(t)$ will be added to adjust the total stress to the yield surface, and then a new self-equilibrated residual stress field is updated again. When the iterative process converges, the residual stress field no longer changes and the evolution of compensation stress $\boldsymbol{\sigma}^{C}(t)$ is also obtained. Thus, the compensation stress can be considered as a symbol for estimating whether the structure shakes down, i.e., whether all the conditions of the static shakedown theorem are satisfied. If the compensation stresses at all Gauss points of the body for every vertex of a load cycle vanish, the structure shakes down.

4 Numerical procedure of the SCM for shakedown analysis

In section 3, the SCM presents an approach to calculating constant residual stress field for shakedown analysis and provides a symbol to estimate whether the structure made up of the elastic-perfectly plastic material shakes down. In this section, an iterative procedure well suitable for shakedown analysis is proposed.

4.1 Evaluation of an initial load multiplier

The numerical procedure starts with an initial load multiplier λ^{ini} and the fictitious elastic stresses $\boldsymbol{\sigma}^{E}(t_i)$. The fictitious elastic stresses $\boldsymbol{\sigma}^{E}(t_i)$ can be obtained via some elastic finite element analyses. An appropriate initial load multiplier λ^{ini} can be calculated

by

$$\lambda^{\mathrm{ini}}=\frac{\int_{\mathrm{V}}\left(\sigma_{\mathrm{y}}\sum_{\mathrm{i}=1}^{\mathrm{NV}}\bar{\varepsilon}_{\mathrm{i}}\right)\mathrm{dV}}{\int_{\mathrm{V}}\left(\sum_{\mathrm{i}=1}^{\mathrm{NV}}\boldsymbol{\sigma}^{\mathrm{E}}\left(\mathrm{t}_{\mathrm{i}}\right)\cdot\boldsymbol{\varepsilon}^{\mathrm{E}}\left(\mathrm{t}_{\mathrm{i}}\right)\right)\mathrm{dV}} \tag{29}$$

where $\boldsymbol{\varepsilon}^{\mathrm{E}}\left(\mathrm{t}_{\mathrm{i}}\right)$ is the elastic stain corresponding to the fictitious elastic stress $\boldsymbol{\sigma}^{\mathrm{E}}\left(\mathrm{t}_{\mathrm{i}}\right)$, and $\bar{\varepsilon}_{\mathrm{i}}$ is the effective strain of $\boldsymbol{\varepsilon}^{\mathrm{E}}\left(\mathrm{t}_{\mathrm{i}}\right)$. Then the value of the initial load multiplier must be bigger than that of the shakedown limit.

4.2 Iterative procedure for shakedown analysis

The numerical procedure is made up of two iteration loops. The inner one controlled by iteration m is used to obtain the compensation stress $\boldsymbol{\sigma}^{\mathrm{C}}\left(\mathrm{t}_{\mathrm{i}}\right)$ at every load vertex and the constant residual stress field for shakedown analysis. The outer one controlled by iteration k is used to update the shakedown load multiplier. The iterative steps are then followed, for the outer iteration k:

(1) Complete all of the steps in the inner loop, which is summarized in Section 3.

(2) Calculate the maximum value of the variable $\xi^{(\mathrm{m+1})}\left(\mathrm{t}_{\mathrm{i}}\right)$ at all the Gauss points for all load vertices at the end of load cycle, that is

$$\xi_{\max}^{(\mathrm{k+1})}=\max\left(\xi^{(\mathrm{m+1})}\left(\mathrm{t}_{\mathrm{i}}\right)\right) \tag{30}$$

(3) The following judgments are examined:

$$\frac{\xi_{\max}^{(\mathrm{k+1})}}{\xi_{\max}^{(\mathrm{k})}}\le \mathrm{tol2},\ \text{and}\ \omega>0.1 \tag{31}$$

where tol2 usually takes 0.1~0.2; the initial value of $\xi_{\max}^{(1)}$ is 1.0; and ω is a convergence parameter with an initial value 0.1~0.5. If Condition (31) holds, the load multiplier is modified by

$$\lambda^{(\mathrm{k+1})}=\frac{\lambda^{(\mathrm{k})}\left(1-\frac{\omega}{2}\cdot\xi_{\max}^{(\mathrm{k+1})}\right)}{\left(1-\omega\cdot\xi_{\max}^{(\mathrm{k+1})}\right)} \tag{32}$$

and then the convergence parameter ω is halved:

$$\omega = \frac{\omega}{2} \tag{33}$$

otherwise, a new load multiplier is calculated by the following expression:

$$\lambda^{(k+1)} = \lambda^{(k)} \left(1 - \omega \cdot \xi_{\max}^{(k+1)}\right) \tag{34}$$

where $\lambda^{(k)}$ is the previous load multiplier; and $\lambda^{(k+1)}$ is the updated load multiplier.

(4) A desired tolerance tol3 is given to estimate whether $\xi_{\max}^{(k+1)}$ approaches to zero or not

$$\xi_{\max}^{(k+1)} \le \text{tol3} \tag{35}$$

(5) Repeat the steps 1~4. If condition (35) is satisfied, the calculated load multiplier becomes the shakedown limit multiplier λ_{sh}, i.e.

$$\lambda^{(k+1)} = \lambda_{sh} \tag{36}$$

otherwise, a new outer iteration starts.

4.3 Convergence and accuracy considerations

A robust and effective iterative control technique and some tolerance parameters are adopted in the numerical procedure to ensure the calculation accuracy and efficiency of the method. Beginning with an initial load multiplier above the shakedown limit, the novel SCM procedure for the shakedown analysis will generate a series of descending load multipliers that converge to the shakedown limit.

The tolerance parameter tol1 used to stop the inner loop, is the key factor to balance the accuracy and efficiency of the algorithm. Small value of tol1 that represents the strict convergence criteria will lead to a more sophisticated calculation of constant residual stress field for shakedown analysis. The calculated shakedown limit multiplier is mainly determined by the finally convergent solution that satisfies the entire conditions of the static shakedown theorem, and has few relations with the solution in the intermediate process where the conditions of the static shakedown theorem are not satisfied. Therefore, the dynamically varying values of tol1, which is large in the beginning of the iterative procedure and becomes smaller with the approaching of load multiplier to shakedown limit multiplier, are adopted to

improve the speed of convergence. A final value of $\mathrm{tol1}=10^{-4}$ turns out to be enough for a good calculation accuracy.

An initial convergence parameter $\omega=0.5$ does not prohibit the load multiplier from overshooting below the target solution at shakedown limit, and hence the numerical scheme shown in Eqs. (31)-(33) is followed to deal with this problem. Then even though the overshooting dose still occur, its value becomes negligible. If Condition (31) is satisfied, the calculated load multiplier will increase till its value exceeds the shakedown limit, and then the iterative procedure goes on. A typical convergence procedure of the SCM for shakedown analysis is illustrated in Fig. 3.

Since that, the adopted shakedown criterion is based on the static shakedown theorem and the entire conditions of the theorem are satisfied when the iterative procedure converges, the calculated shakedown limit multiplier will be a lower bound to the actual shakedown solution. In fact, the criterion in Eq. (35) is equivalent to the following form:

$$\left|\frac{\lambda^{(\mathrm{k}+1)}-\lambda^{(\mathrm{k})}}{\lambda^{(\mathrm{k})}}\right| \le \omega \cdot \xi_{\max}^{(\mathrm{k}+1)} \tag{37}$$

Because the value of ω is no more than 0.5, the relative error of the calculated shakedown limit multiplier is no more than 0.1%.

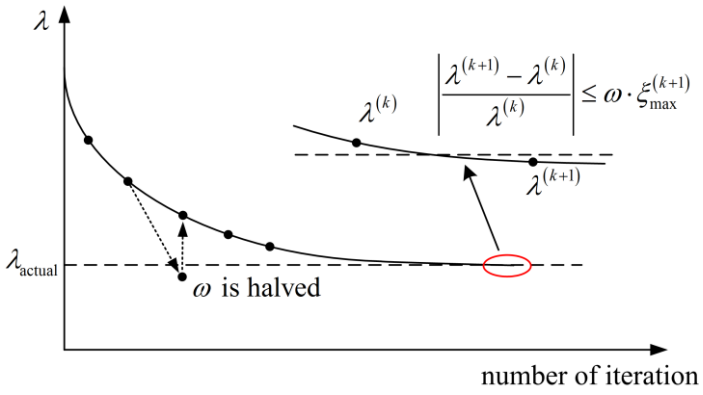

Fig. 3. Typical convergence procedure of the SCM for shakedown analysis.

5 Numerical applications

In this section, three different numerical examples of shakedown analysis for structures under mechanical and thermal loads that vary within multi-dimensional loading domain are

considered. The presented algorithm is implemented into the commercial finite element software ABAQUS [47] via user subroutine UMAT and is used to calculate the shakedown limits of these structures.

All the structures are made up of homogeneous, isotropic and elastic-perfectly plastic material with von Mises yield surface. The material parameters are assumed independent of the applied temperature and constant with time. All the calculations are carried out on the personal computer with 16GB RAM and Intel Core i7 at 3.39GHz.

5.1 Bree problem

The first example is the Bree problem [37, 40, 46, 48, 49], which is a common benchmark example of shakedown analysis for structures under mechanical and thermal loads. As illustrated in Fig. 4, the thin plate is subjected to a tension σ_{p} and a temperature difference $\Delta\theta(\mathrm{t})$ that is linearly distributed along the width of the plate, and the deformation due to the thermal gradient is restrained by boundary constraints. The tension σ_{p} and the temperature difference $\Delta\theta(\mathrm{t})$ may vary in three different loading paths, as shown in Fig. 5. The finite element model of the plate consists of 630 8-node quadratic plane stress elements (ABAQUS CPS8) with 3×3 Gauss integration points. The material properties of the plate are given in Table 1.

The plane stress Bree cases considering two loading paths (Fig. 5a and b) have been studied numerically and analytically by some authors [40, 49], and the two loading paths correspond to two types (Type-I and Type-II) of the Bree problem. Here, three different loading paths are considered for the purposes of comparison and verification.

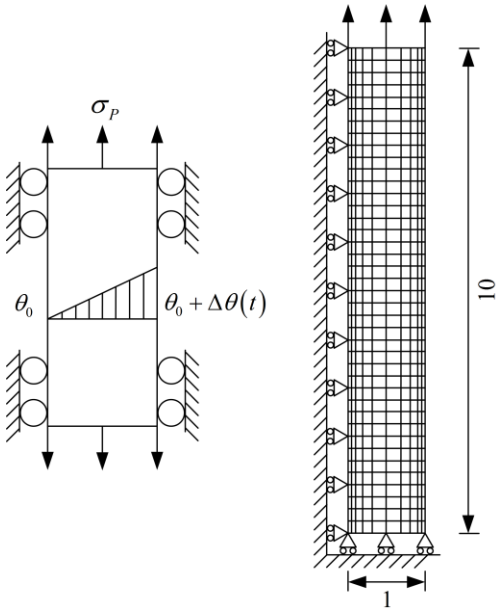

Fig. 4. Geometry and finite element model for the Bree problem.

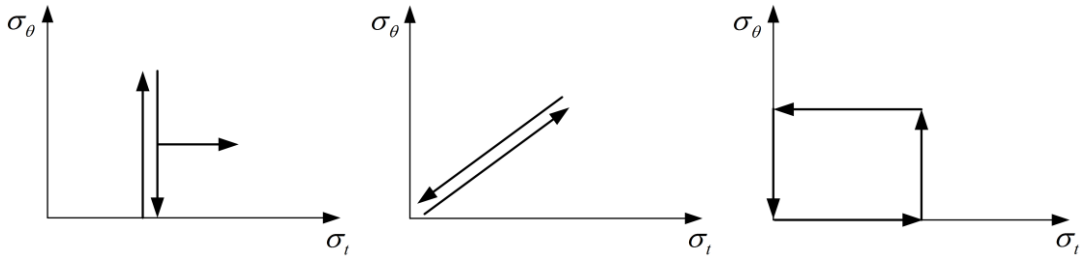

a Type-I **b** Type-II **c** Type-III

Fig. 5. Three loading paths for the Bree problem.

Table 1 Material properties of the thin plate.

Young's modules E	Poisson's ratio v	Yield stress ..	Coefficient of thermal expansion α
208 GPa	0.3	360 MPa	5×10^{-5} /℃

5.1.1 Type-I

The first type (Type-I) is the classic Bree problem, where the thermal load is cyclic and the mechanical load is constant. The analytical solution of the classic Bree problem for von Mises yield criterion has been provided by Bree [48], and the shakedown boundary can be determined by two straight-line segments (Fig. 6), that is

$$\begin{aligned} \frac{\sigma_\theta}{\sigma_{\mathrm{y}}} &= 2 \qquad && \forall\ 0 \le \frac{\sigma_{\mathrm{p}}}{\sigma_{\mathrm{y}}} \le \frac{1}{2} \\ \frac{\sigma_{\mathrm{p}}}{\sigma_{\mathrm{y}}} + \frac{1}{4}\frac{\sigma_\theta}{\sigma_{\mathrm{y}}} &= 1 \qquad && \forall\ \frac{1}{2} < \frac{\sigma_{\mathrm{p}}}{\sigma_{\mathrm{y}}} \le 1 \end{aligned} \tag{38}$$

where σ_θ is the maximum thermal elastic stress due to the fluctuating temperature difference $\Delta\theta(\mathrm{t})$.

The SCM is used to calculate shakedown limits of the plate under various ratios of the constant tension and the fluctuating temperature difference. As a result, the corresponding numerical results are displayed in Fig. 6, where the tension σ_{p} and the maximum thermal stress σ_θ are normalized by the uniaxial yield stress.

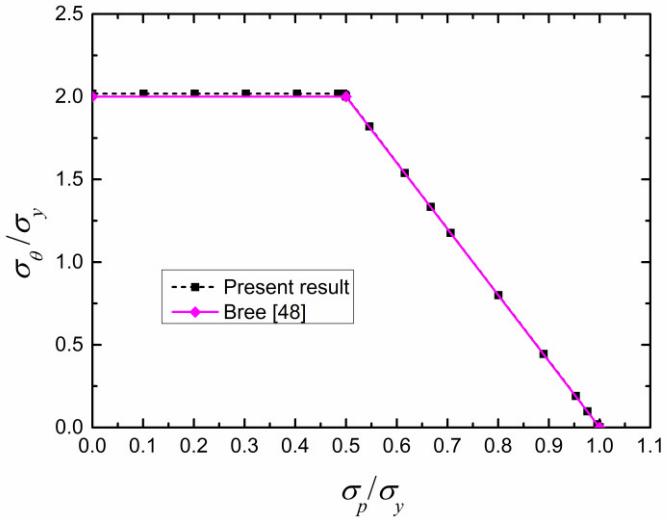

Fig. 6. Shakedown limits calculated by the SCM and its comparison with the analytical solution by Bree [48] for Type-I Bree problem.

It can be seen from Fig. 6 that the numerical results by the SCM are in good agreement with the analytical solution, apart from some slight differences in the segment where $\sigma_{\mathrm{p}}/\sigma_{\mathrm{y}}$ ranges from 0.0 to 0.5. This segment just corresponds to the alternating plasticity region of shakedown boundary. The slight differences can be explained with the failure mechanism of the structure when it fails to shake down. If the alternating plasticity mechanism is decisive for shakedown, the maximum stress point in the structure will dominate the shakedown limit. The maximum stress points are located on the edges of the plate in this case; however, there is

404 no Gauss points on them. The stress via the finite element calculation will be slightly lower
405 than the actual stress at the edge. Thus, the computed shakedown limit by the SCM is slightly
406 higher than the analytical solution in the alternating plasticity region. This merely
407 demonstrates that the difference is due to the finite element solution. If the finite element
408 discretization is finer, we will obtain a nearer solution to the exact one.

409 5.1.2 Type-II

410 The second type (Type-II) is the modified Bree problem, where the thermal load and the
411 mechanical load vary proportionally. The analytical solution of the Type-II Bree problem for
412 von Mises yield criterion has been obtained by Bradford [49], and the shakedown boundary
413 shown in Fig. 7 can be determined by

414
$$\begin{aligned} \frac{\sigma_\theta}{\sigma_{\mathrm{y}}}+\frac{\sigma_{\mathrm{p}}}{\sigma_{\mathrm{y}}}=2 \qquad & \forall\, 1\le\frac{\sigma_\theta}{\sigma_{\mathrm{y}}}\le 2 \\ \frac{\sigma_{\mathrm{p}}}{\sigma_{\mathrm{y}}}=1 \qquad & \forall\, 0\le\frac{\sigma_\theta}{\sigma_{\mathrm{y}}}\le 1 \end{aligned} \tag{39}$$

415 The SCM is used to calculate the shakedown boundary of the Type-II problem, and the
416 corresponding numerical results are displayed in Fig. 7. That the maximum relative error
417 between the numerical results and the analytical solutions is no more than 0.9% demonstrates
418 the good accuracy of the SCM.

419
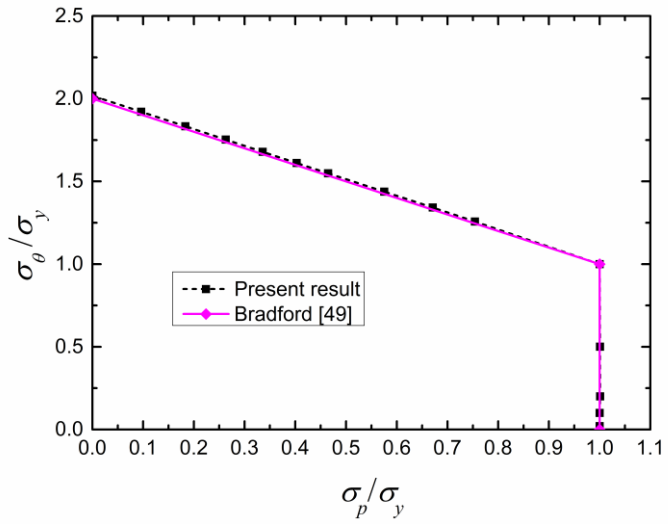

420 **Fig. 7.** Shakedown limits calculated by the SCM and its comparison with the analytical
421 solution by Bradford [49] for Type-II Bree problem.

5.1.3 Type-III

The third type (Type-III) is another modified Bree problem, where the thermal load and the mechanical load vary independently. Fig. 8 shows the numerical results of the shakedown analysis by the SCM.

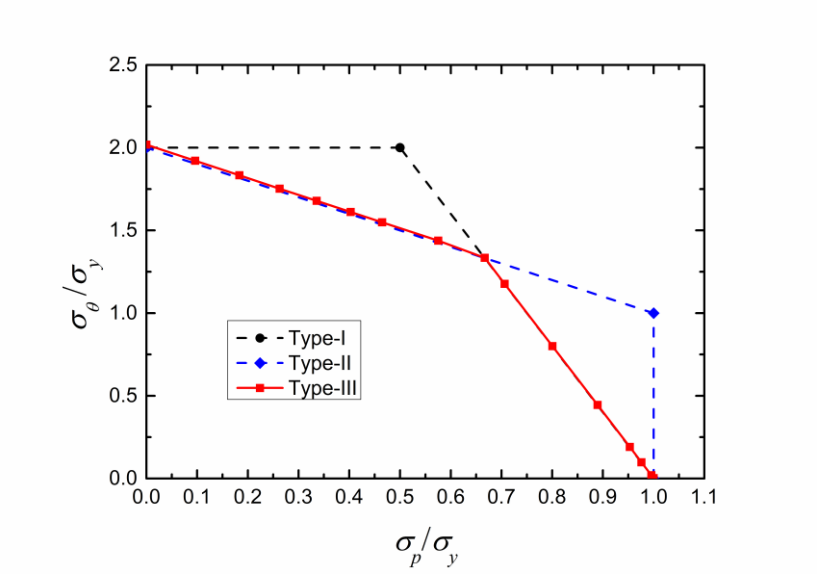

Fig. 8. Shakedown limits calculated by the SCM for Type-III Bree problem.

It can be seen from Fig. 8 that the shakedown boundary of the Type-III Bree problem is the lower envelope of the shakedown boundaries of the Type-I Bree problem and the Type-II Bree problem. Therefore, a more stringent shakedown domain can be obtained when the mechanical and thermal loads vary independently in a rectangle loading domain. Thus, the loading condition of structural components must be assessed carefully in practical engineering design.

For the three types of the Bree problems above, the procedures of the SCM for shakedown analysis all present good convergence and the numerical results are in good agreement with these analytical solutions. A typical iterative convergence process of the shakedown multiplier λ for the load combination $\sigma_{\mathrm{p}}=0$ is depicted in Fig. 9, where the horizontal line segment indicates that the procedure of the SCM is being carried out in its inner iterative loop and the jump point indicates the procedure of the SCM is being carried out in its outer iterative loop. As a result, the y-axial component residual stress field of the plate is displayed in Fig. 10 when the shakedown limit reaches.

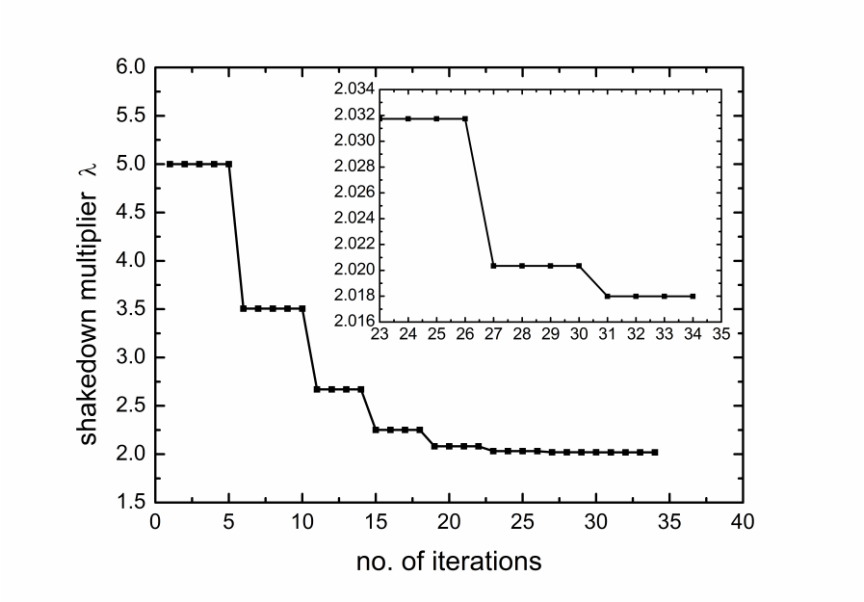

Fig. 9. A typical iterative convergence process of the shakedown multiplier for the Bree problem.

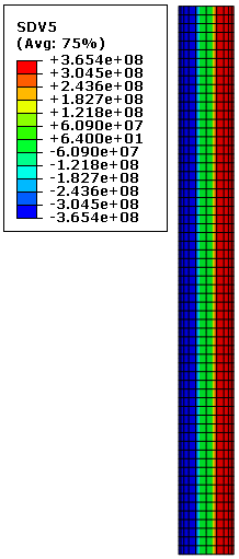

Fig. 10. Y-axial component residual stress field of the plate.

5.2 Square plate with a central circular hole

Tube sheets are usually used as supporting elements in heat exchangers and boilers. When heated fluid passes through the tubes, the tube sheets undergo temperature difference, which may cause thermal stresses in their bodies. The representative cell including a square plate with a central circular hole (Fig. 11) is established to investigate the load-carrying capability of tube sheets under variable mechanical and thermal loads.

Due to the symmetry of the structure and the loading, only one quarter of the holed plate is considered. The geometry of the structure and its quarter finite element model are shown in Fig. 11. The ratio between the diameter D of the circular hole and the length L of the square plate is 0.2. The ratio between the thickness d of the plate and its length L is 0.05. The mesh discretization consists of 432 8-node quadratic plane stress elements (ABAQUS CPS8) with 3×3 Gauss integration points. The material properties of the plate are the same as those given in Table 1.

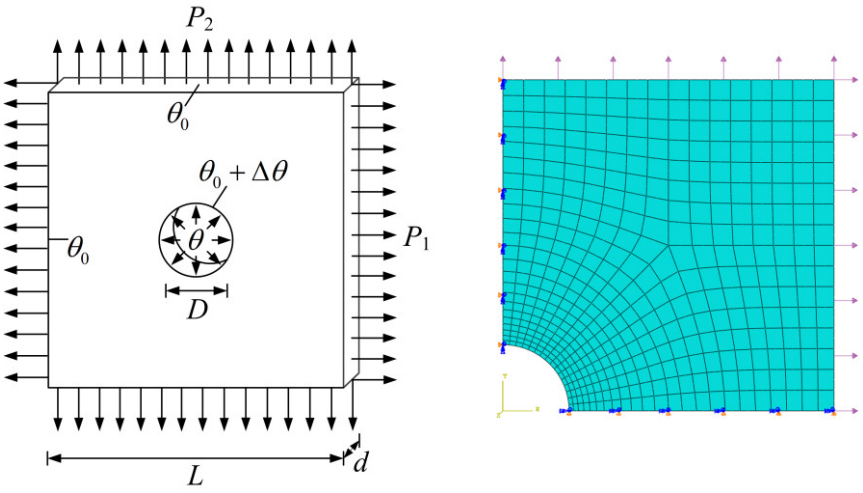

Fig. 11. Geometry of the holed plate and its quarter finite element model.

The plate is subjected to three loads that consist of a temperature difference $\Delta\theta(\mathrm{t})$ between the edge of the hole and the outer edge of the plate, and two uniform normal tractions P_1 and P_2 at the vertical edge and the horizontal edge of the plate respectively. For the convenience of comparison, the variation of the temperature with radius r is assumed the same distribution as in [39, 46]:

$$\theta=\theta_0+\Delta\theta\frac{\ln\left(5\frac{\mathrm{D}}{2}\Big/\mathrm{r}\right)}{\ln(5)} \tag{40}$$

which is an approximation to the temperature field corresponding to $\theta=\theta_0+\Delta\theta$ at the edge of the hole and $\theta=\theta_0$ around the outer edge of the plate.

For the calculations of different initial elastic stress fields, $\mathrm{P}_1^*=\mathrm{P}_2^*=360\mathrm{MPa}$, $\theta_0=0$ and $\Delta\theta^*=90.2℃$ have been adopted. The maximum von Mises stress at the edge of the holed plate due to the thermal load is σ_θ. In order to test and verify the reliability of the

proposed procedure for shakedown analysis of the plate under multiple mechanical and thermal loads, three different loading conditions have been considered here.

(1) Case I

We consider that the three loads vary independently in the following ranges:

$$\begin{aligned} 0 \le \mathrm{P}_1 \le \mu_1 \mathrm{P}_1^* \\ 0 \le \mathrm{P}_2 \le \mu_2 \mathrm{P}_2^* \\ 0 \le \Delta\theta \le \mu_3 \Delta\theta^* \end{aligned} \tag{41}$$

Then the loading domain becomes a cuboid in the space of load parameters, as shown in Fig. 12a. Considering the different ratios among μ_1, μ_2 and μ_3, 111 load combinations in the three-dimensional loading space are chosen for shakedown analysis of the plate, as illustrated in Fig. 12b.

(2) Case II

Here we consider that the mechanical load P_1 keeps constant, and the mechanical load P_2 and the thermal load vary independently, that is

$$\begin{aligned} \mathrm{P}_1 = \mu_1 \mathrm{P}_1^* \\ 0 \le \mathrm{P}_2 \le \mu_2 \mathrm{P}_2^* \\ 0 \le \Delta\theta \le \mu_3 \Delta\theta^* \end{aligned} \tag{42}$$

Then the loading domain becomes a plane in the space of load parameters, as shown in Fig. 12c. In order to depict the shakedown domain clearly, 205 load combinations in the three-dimensional loading space are chosen for shakedown analysis of the plate, as illustrated in Fig. 12d. It is worth noting that the blue line plotted in Fig. 12d denotes these load combinations of $\mu_2/\mu_1 = 0.761$.

(3) Case III

Now we consider that the mechanical loads P_1 and P_2 keep constant, and the thermal load varies, that is

$$\begin{aligned} \mathrm{P}_1 = \mu_1 \mathrm{P}_1^* \\ \mathrm{P}_2 = \mu_2 \mathrm{P}_2^* \\ 0 \le \Delta\theta \le \mu_3 \Delta\theta^* \end{aligned} \tag{43}$$

Then the loading domain becomes a line in the space of load parameters, as shown in Fig. 12e. 122 load combinations in the three-dimensional loading space are chosen for shakedown

analysis of the plate, as illustrated in Fig. 12f.

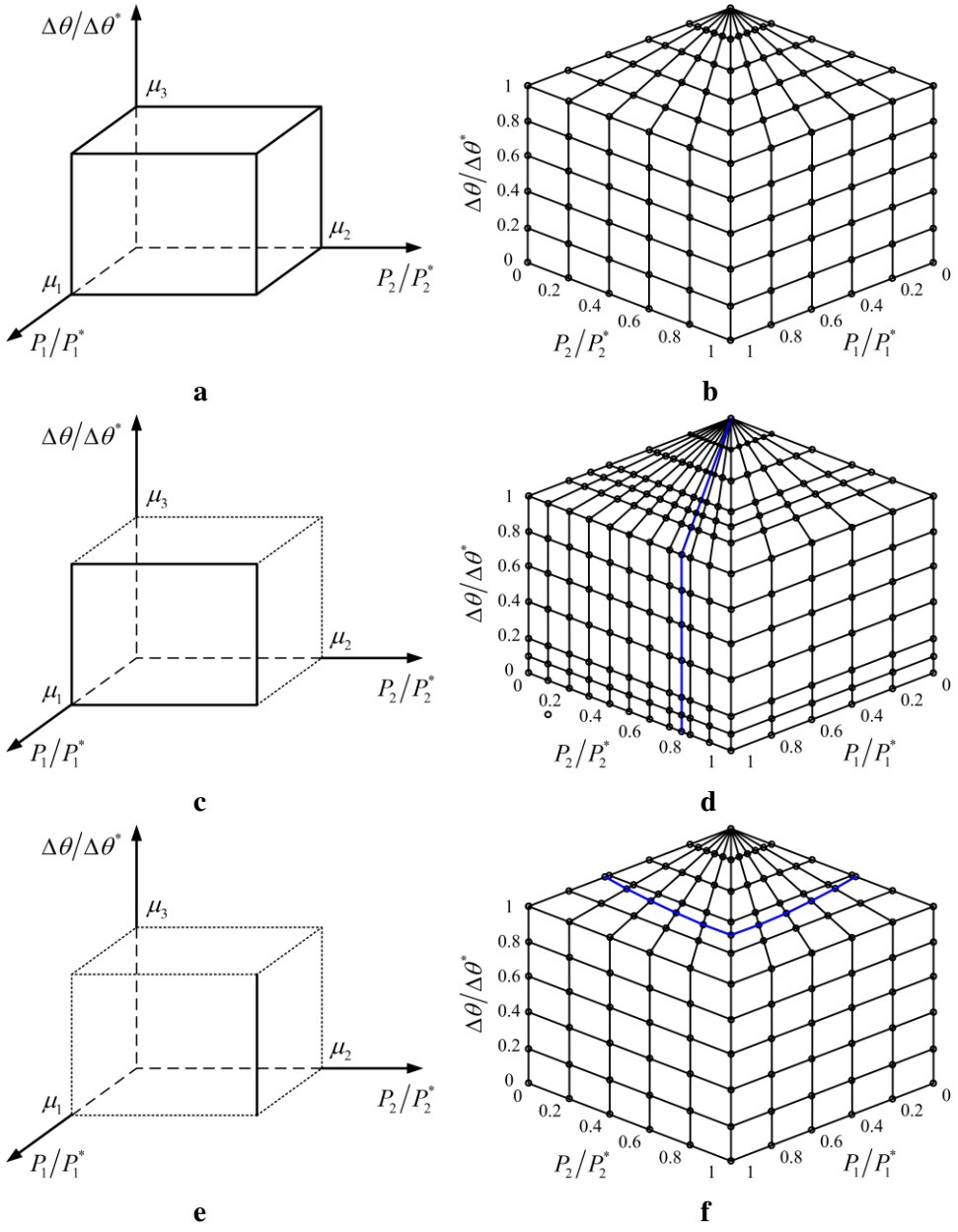

Fig. 12. Loading domain and computed load combinations in loading space.

The proposed algorithm is adopted to calculate the shakedown limits of the plate for the three cases. Fig. 13a, b and c show the three-dimensional shakedown domains of the plate for case I, case II and case III, respectively.

From Fig. 13a, one can observe that the 111 shakedown limit points are located in two intersecting planes, i.e., the plane A-B-C and the plane B-C-D. It is worth noting that the shakedown limit points in these two planes are both dominated by alternating plasticity mechanism. From Fig. 13b, it can be seen that the shakedown boundaries consist of the plane

B-C-D-E and the surface A-B-E, and that the shakedown domain expands comparing to that in Fig. 13a. Moreover, the blue line B-D in Fig. 13b denotes the shakedown limits corresponding to the load combinations of $\mu_2/\mu_1=0.761$, which are plotted as blue line in Fig. 12d. It is worth noting that the shakedown limit points in the plane B-C-D-E are dominated by alternating plasticity mechanism, and the points in the surface A-B-E are dominated by ratcheting mechanism. From Fig. 13c, one can observe that the shakedown boundaries consist of two surfaces A-B-E-D, B-C-F-E and the plane D-E-F-G, and the shakedown domain further expands comparing to that in above two cases. It should be noted that the shakedown limit points in the plane D-E-F-G are dominated by alternating plasticity mechanism, and the points in both the surface A-B-E-D and the surface B-C-F-E are dominated by ratcheting mechanism.

In order to verify the failure mechanism that dominates the shakedown boundaries of the plate for different cases, several individual step-by-step incremental elastic-plastic calculations are conducted, as depicted by the red, black and blue markers with capital letters M, N and P in Fig. 13b and c. In both Fig. 13b and Fig. 13c, the load combination marked with red "M" indicates shakedown behavior, while the load combination marked with black "N" indicates alternating plasticity behavior and the red load combination marked with blue "P" illustrates ratcheting behavior. As results, details relating to the effective plastic strains over the first 15 load cycles at a Gauss point of the plate from the load combinations M, N and P (Fig. 13b) are displayed in Fig. 14. Fig. 15 shows the effective plastic strains over the first 30 load cycles at a Gauss point of the plate from the three load combinations M, N and P (Fig. 13c). These results illustrate that the three load combinations M, N and P depicted in both Fig. 13b and Fig. 13c exhibit shakedown, alternating plasticity and ratcheting behavior, respectively. The results from step-by-step incremental elastic-plastic analysis clearly reveal the different failure mechanisms of the plate under various load combinations.

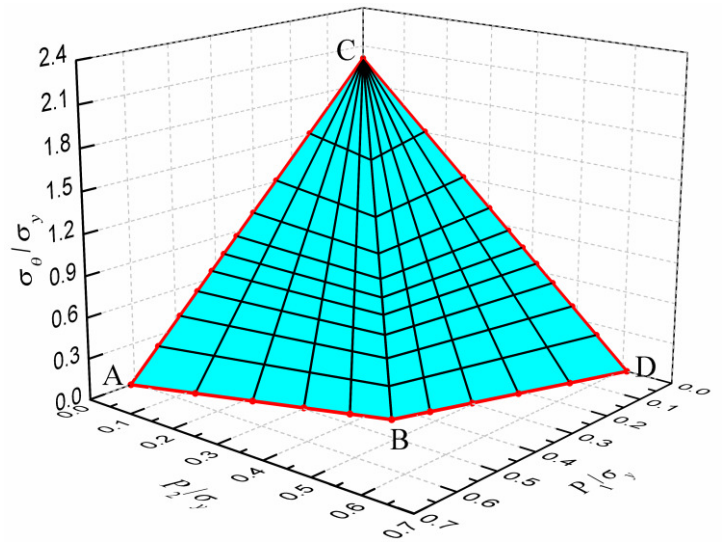

537

538 **a** for case I

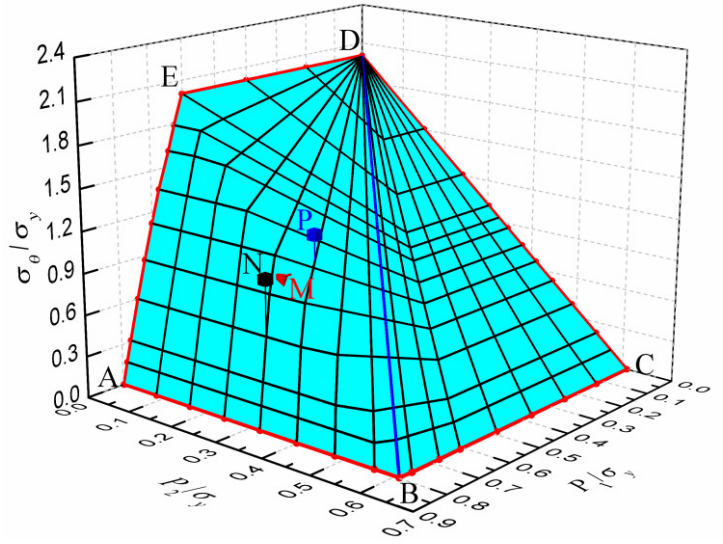

539

540 **b** for case II

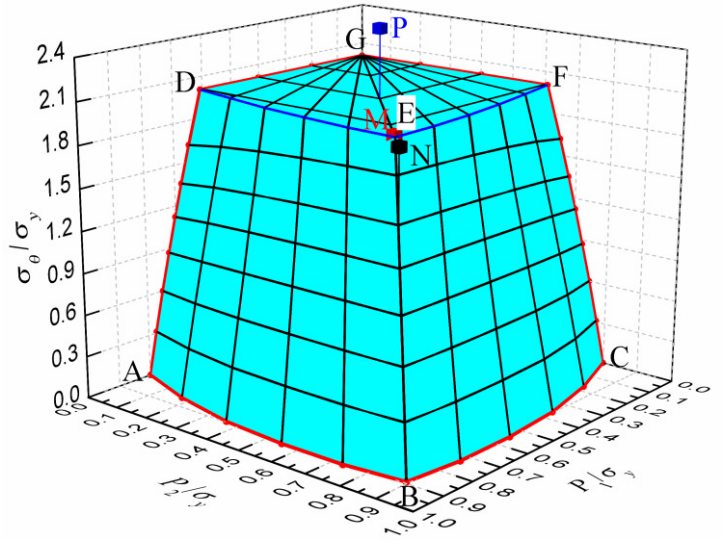

541

542 **c** for case III

543 **Fig. 13.** Shakedown domain of the plate in three-dimensional loading space.

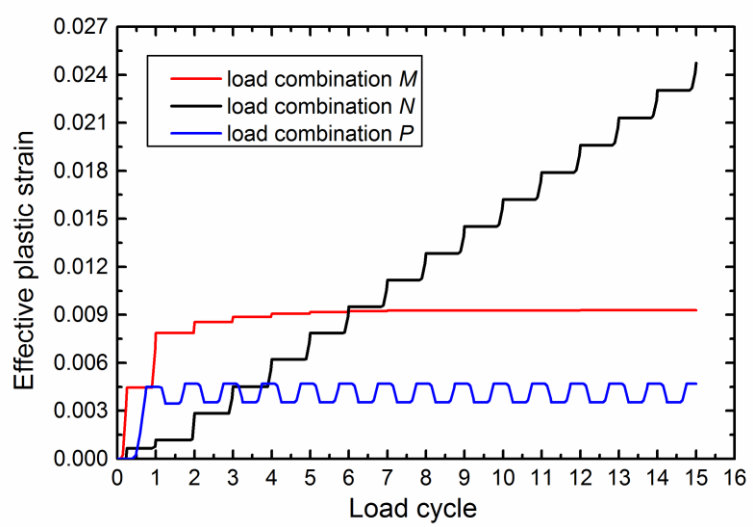

Fig. 14. Effective plastic strains over the first 15 load cycles at a Gauss point of the plate from load combinations M, N and P for case II.

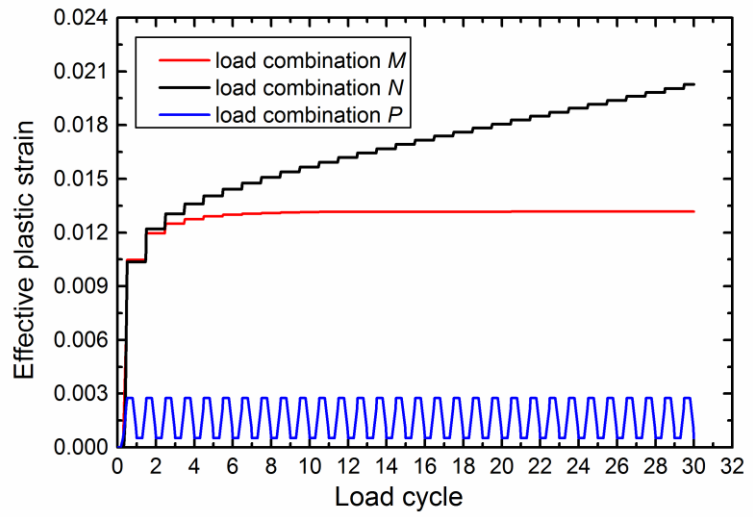

Fig. 15. Effective plastic strains over the first 30 load cycles at a Gauss point of the plate from load combinations M, N and P for case III.

To describe quantitatively these shakedown domains of the plate, numerical results of shakedown analysis for some typical computed load combinations are given in Table 2. It is worth noting that these calculated shakedown limits are marked with capital letters in Fig. 13.

Assuming that one of the loads is equal to zero, the three-dimensional loading space degenerates into the two-dimensional loading space. Then the shakedown limit points will be presented as two-dimensional plot. Fig. 16a shows the shakedown domains of the plate in two-dimensional loading space when the thermal load vanishes for the three cases considered above. Fig. 16b shows the shakedown domains of the plate in two-dimensional loading space

when the mechanical load P_2 vanishes for the three cases considered above.

Table 2 Numerical results of shakedown analysis in three-dimensional loading space.

Computed load combination	Shakedown limit (P_1/σ_y , P_2/σ_y , σ_θ/σ_y)		
	Case I	Case II	Case III
A	(0.609, 0, 0)	(0.798, 0, 0)	(0.798, 0, 0)
B	(0.442, 0.442, 0)	(0.798, 0.608, 0)	(0.894, 0.894, 0)
C	(0, 0, 2.002)	(0, 0.609, 0)	(0, 0.798, 0)
D	(0, 0.609, 0)	(0, 0, 2.002)	(0.608, 0, 2.002)
E	----	(0.608, 0, 2.002)	(0.685, 0.685, 2.002)
F	----	----	(0, 0.608, 2.002)
G	----	----	(0, 0, 2.002)

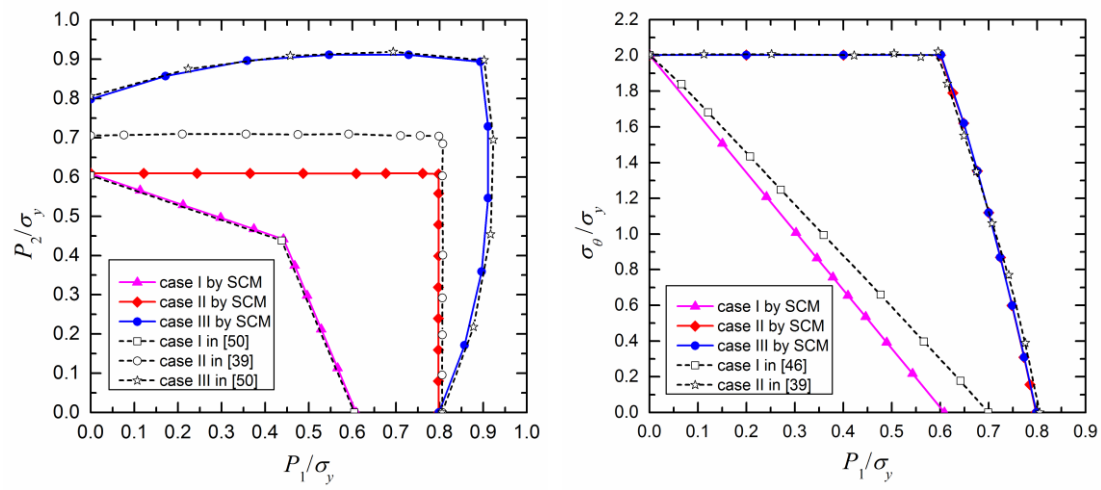

a thermal load vanishes **b** mechanical load P_2 vanishes

Fig. 16. Shakedown domains of the plate in two-dimensional loading space.

As a typical example, the shakedown analysis of the holed plate under two loads has been studied by several authors [28, 30, 39, 46, 50]. For the comparison purpose, some results from [39, 46, 50] are plotted in Fig. 16 additionally. From Fig. 16a, we can observe that the present results are in good agreement with the solutions from [50] but have some differences with these from [39]. It should be stated that the discrepancy of the shakedown limits between our results and these from [39] is mainly due to the different mesh discretization. From Fig. 16b, we can observe that the present results are in good agreement with these from [39] but have some differences with these from [46]. The slight discrepancy of the shakedown limits

between our results and these from [46] is also due to the different mesh discretization.

5.3 Thick vessel with nozzles

The third example is a thick vessel with nozzles, which is the key part of nuclear reactor plant. One quarter of the geometric model is shown in Fig. 17. During the regular operation, the reactor plant works under steady temperature and pressure. However, the vessel will be subjected to a large temperature gradient and varying pressure while the reactor plant shuts down, starts up or undergoes abnormal operating cases. In order to conveniently simulate the cyclic process of the start-up, shutdown and abnormal operating case during the whole service, we assume that the temperature history $\theta(\mathrm{t})=\theta_0+\Delta\theta(\mathrm{t})$ on the inside surface of the vessel with nozzles follows the curve in Fig. 18 and the internal pressure varies in the range $\mathrm{P}\in[0,\mathrm{P}_0]$. Due to the insulation treatment, the outside surfaces of the vessel and the nozzles sustain constant temperature. The initial temperature of the structure and the environment temperature are both $\theta_0=20$ ℃. It is worth noting that the constant temperature period of the temperature history depicted in Fig. 18 is long enough for the reactor plant to reach the steady operation state.

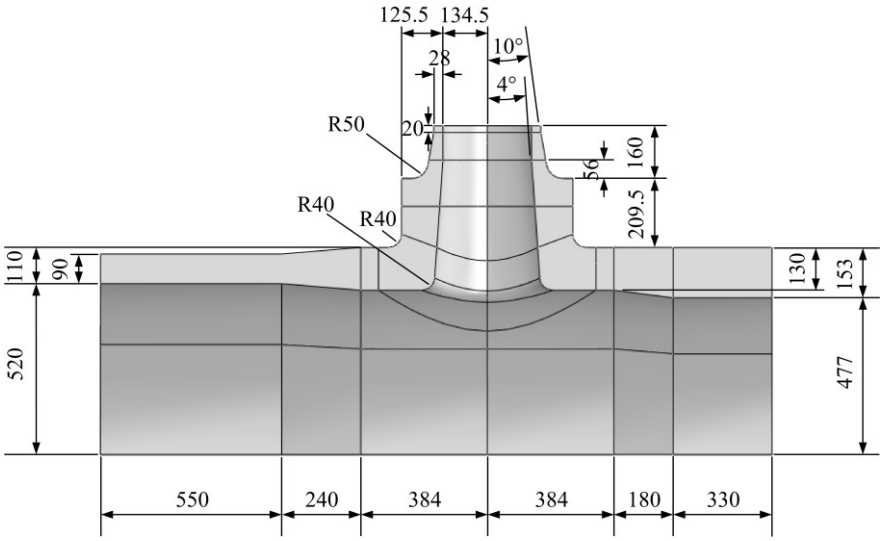

Fig. 17. Geometric model of the thick vessel with nozzles.

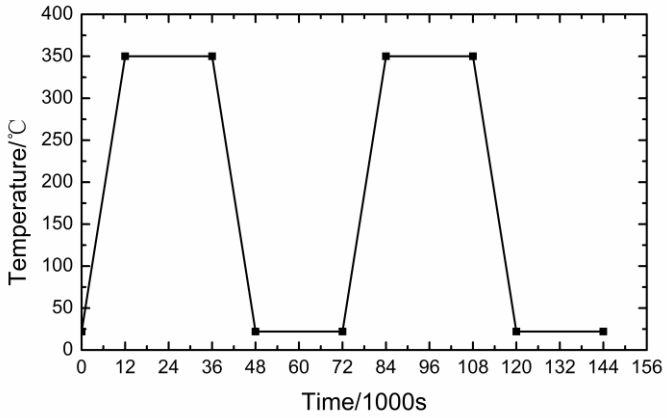

Fig. 18. Temperature history on the inside surface of the vessel and the nozzles.

Considering the symmetry of the structure and the loading, only one quarter of the thick vessel with nozzles is established. Fig. 19 shows the finite element model of the structure, where the symmetric boundary conditions are used and the forces acting on the ends of the vessel and nozzles are replaced with the equivalent uniformly distributed tensions to consider closed end condition. In order to optimize the efficiency and accuracy of the calculation, the finite element meshes around the stress concentration areas are refined properly. The mesh discretization consists of 3358 elements and 16655 nodes. In calculations, the 20-node quadratic brick elements (ABAQUS C3D20D) are used for the determination of the temperature distribution and the 20-node quadratic brick elements with reduced integration (ABAQUS C3D20R) are used for the structural stress analysis.

The material properties of the vessel with nozzles are given in Table 3.

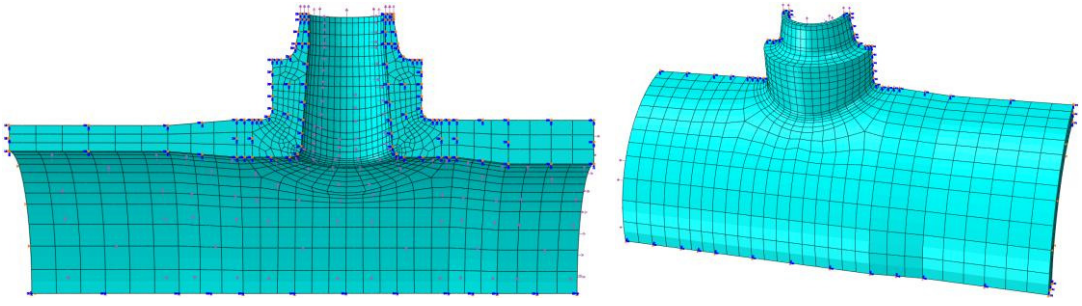

Fig. 19. Finite element model of the thick vessel with nozzles.

606 **Table 3** Material properties of the thick vessel with nozzles.

Young's modules E	2.1×10^5 MPa
Poisson's ratio v	0.3
Yield stress σ_y	200 MPa
Density ρ	8100 kg/m^3
Thermal conductivity	18 W/(m℃)
Specific heat capacity	430 J/(kg℃)
Coefficient of thermal expansion α	1.8×10^{-5}

607

608 5.3.1 Heat transfer analysis and elastic stress calculation

609 First, the transient heat transfer analysis is carried out to calculate the temperature field
610 history of the entire body. As a result, temperature histories of nodes 1282 and 1345 are
611 shown in Fig. 20, each of which represents a node on the inside or the outside surface of the
612 vessel respectively. Then the structural stress analysis is followed to calculate the thermal
613 elastic stress field and the mechanical elastic stress field. The dangerous moments for the
614 vessel with nozzles under thermal load are at 12000 s and 48000 s, which are just the final
615 moments of the start-up and the shutdown respectively. Fig. 21a and b show the temperature
616 field distributions of the vessel with nozzles at 12000 s and 48000 s, respectively. The
617 corresponding von Mises elastic stress fields are displayed in Fig. 22a and b, respectively. It
618 should be noted that although the distributions of von Mises elastic stress field in Fig. 22a and
619 b are the same, the directions of stress fields at 12000 s and 48000 s are opposite, and thus the
620 structure suffers from the maximum stress range between the two moments. The von Mises
621 elastic stress field of the vessel with nozzles under internal pressure is shown in Fig. 23.

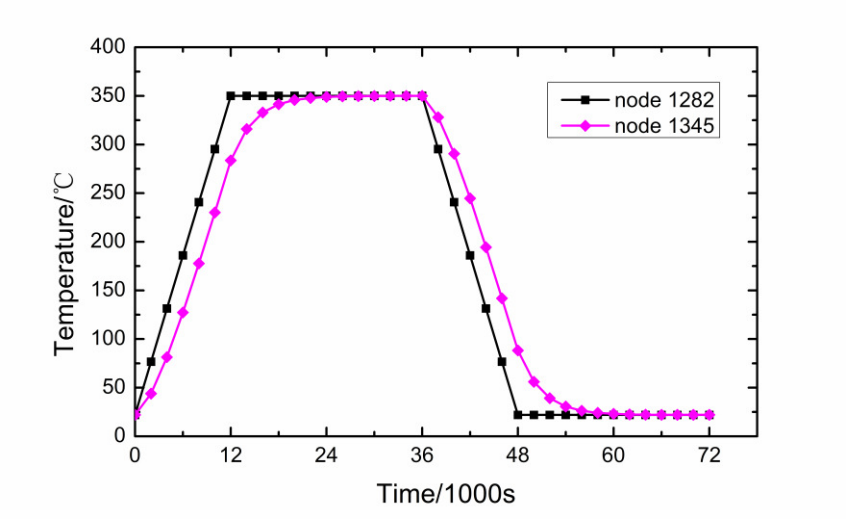

Fig. 20. Temperature histories of nodes 1282 and 1345.

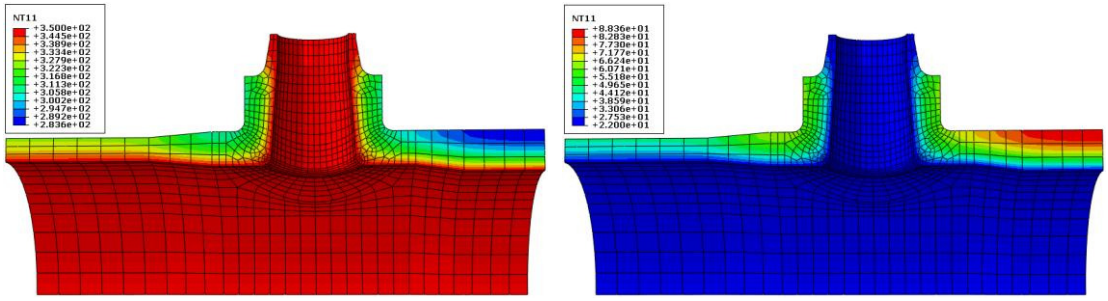

a at 12000 s **b** at 48000 s

Fig. 21. Temperature distributions of the thick vessel with nozzles.

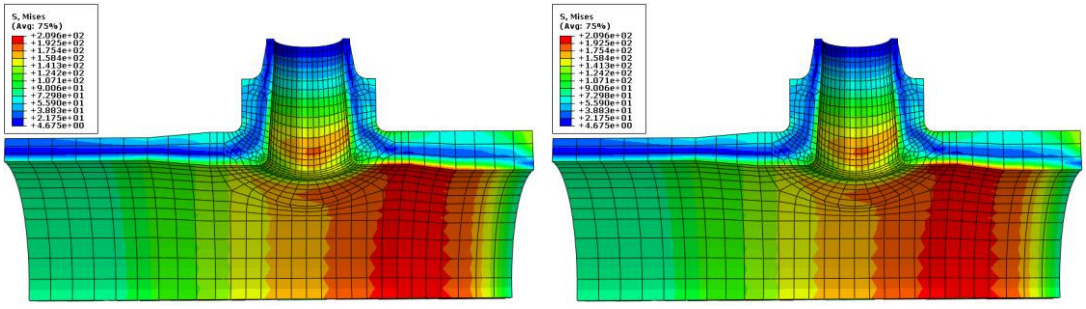

a at 12000 s **b** at 48000 s

Fig. 22. Von Mises elastic stress field of the thick vessel with nozzles under thermal load.

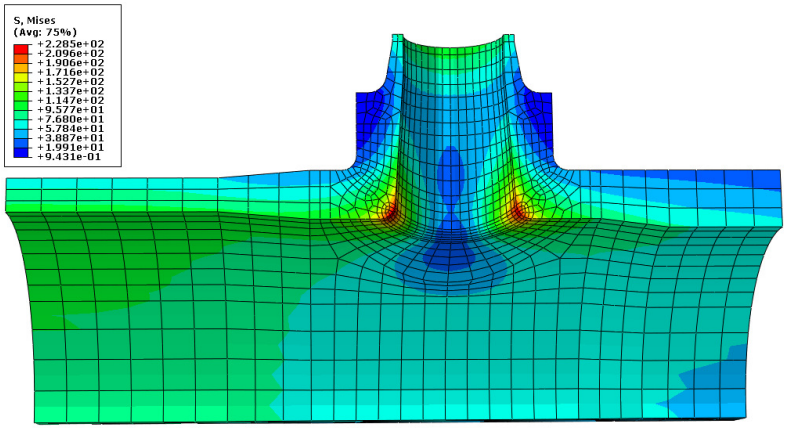

Fig. 23. Von Mises elastic stress field of the thick vessel with nozzles under internal pressure.

5.3.2 Shakedown analysis

The SCM is used to calculate the shakedown limit of the thick vessel with nozzles. Considering the randomness of the varying temperature gradient and internal pressure, four vertices are used to define the loading domain (Fig. 24), which include two instants for thermal load at t = 12000 and 48000 s and two instants for pressure load at P = 0 and 15.5 MPa. The applied total elastic stress history consists of thermal and pressure components: σ_{θ_0} is the von Mises elastic thermal stress which is associated with the current thermal load θ_0, and σ_{P_0} is the von Mises elastic stress corresponding to the internal pressure $\mathrm{P}_0 = 15.5\,\mathrm{MPa}$. The load multiplier λ is determined so that $\lambda\sigma_{\theta_0}$ and $\lambda\sigma_{\mathrm{P}_0}$ become the shakedown limit, for various proportions of the two components. For the simplicity of description, the angle φ ranging from 0° to 90° is introduced to denote the different proportions of the two stress components.

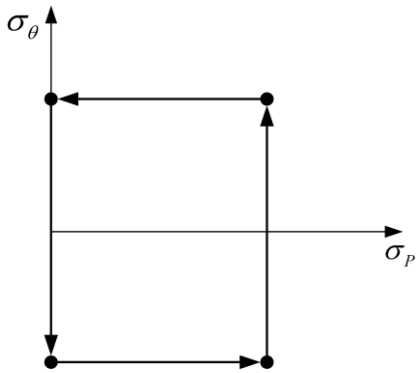

Fig. 24. Loading domain and its vertices.

On basis of the previously calculated elastic stress fields (Fig. 22 and Fig. 23), the shakedown limit multipliers λ are computed for different angles φ in two-dimensional loading space considering the thermal load σ_θ and mechanical load σ_{P} varying independently. The numerical results of the shakedown analysis by the SCM as well as the corresponding computing time are all listed in Table 4. The shakedown domain of the thick vessel with nozzles is shown in Fig. 25.

The shakedown boundary curve is defined by three segments with the intersection points at $\varphi = 30°$ and $\varphi = 56°$, which are plotted in Fig. 25 additionally. It is worth noting that the three segments of shakedown boundary are all dominated by alternating plasticity mechanism, and the difference is due to the different locations of the maximum von Mises stress point.

Under various combinations of the mechanical and thermal loads, all the calculations by the SCM for shakedown analyses of the thick vessel with nozzles present good convergence. As an example, Fig. 26 depicts the iterative convergence process of the shakedown multiplier for the load combination $\sigma_\theta/\sigma_{\theta_0} = \sigma_{\mathrm{P}}/\sigma_{\mathrm{P}_0}$ which corresponds to $\varphi = 45°$. It is worth noting that although the procedure initiates at a relatively high load multiplier, the load multiplier decreases rapidly to a steady value, and then it approaches smoothly to the shakedown limit. Moreover, the von Mises residual stress field of the thick vessel with nozzles for this case is shown in Fig. 27 when the shakedown limit reaches.

According to the conclusions in [12], the shakedown limit of the thick vessel with nozzles is the minimum one of its plastic limit and its double elastic limit when the system is subjected to the single internal pressure. For the applied internal pressure P_0 = 15.5 MPa, the maximum von Mises elastic stress occurs at the corner of the vessel with nozzles (Fig. 23) and its value is 217.9 MPa. Therefore, the corresponding shakedown limit multiplier λ (according to double elastic limit criterion) under the internal pressure is calculated as follows:

$$\lambda = \frac{2 \times 200\mathrm{MPa}}{217.9\mathrm{MPa}} = 1.836 \tag{44}$$

The value is in excellent agreement with the numerical result by the SCM, which has the same load multiplier 1.836. This also indicates that the alternating plasticity mechanism is decisive for the failure of the thick vessel with nozzles under the single internal pressure.

675 In order to evaluate the computational efficiency of the novel SCM for shakedown
676 analysis, the CPU time to calculate shakedown limit of the thick vessel with nozzles under
677 load combination $\sigma_{\mathrm{P}}/\sigma_{\mathrm{P}_0}=\sigma_{\theta}/\sigma_{\theta_0}$ by the SCM, the linear matching method (LMM) [38]
678 and the step-by-step analysis are compared in Table 5. It can be seen from Table 5 that, with
679 necessary accuracy of these calculations, the CPU time by the step-by-step analysis is more
680 than 40 times that by the SCM while the CPU time by the LMM is about 3 times that by the
681 SCM. The usage of the SCM is much cheaper and more efficient than the LMM and the
682 step-by-step analysis.

683 **Table 4** Numerical results and computing time for the shakedown analysis of the thick vessel
684 with nozzles.

φ	$\sigma_{\mathrm{P}}/\sigma_{\mathrm{P}_0}$	$\sigma_{\theta}/\sigma_{\theta_0}$	CPU time (s)
0°	1.836	0	190
5°	1.671	0.146	193
10°	1.531	0.270	211
15°	1.410	0.378	187
20°	1.301	0.474	190
25°	1.203	0.561	186
30°	1.112	0.642	209
35°	1.021	0.715	199
40°	0.934	0.784	195
45°	0.851	0.851	185
50°	0.768	0.915	187
55°	0.687	0.981	188
56°	0.669	0.992	160
60°	0.586	1.014	156
70°	0.388	1.066	151
80°	0.196	1.113	130
90°	0	1.160	128

685

686

687 **Table 5** Comparison of the CPU time by the SCM, the LMM and the step-by-step analysis.

Method	Shakedown limit multiplier	CPU time (s)
The SCM	0.851	185
The LMM	0.859	642
The step-by-step analysis	0.853	7758

688

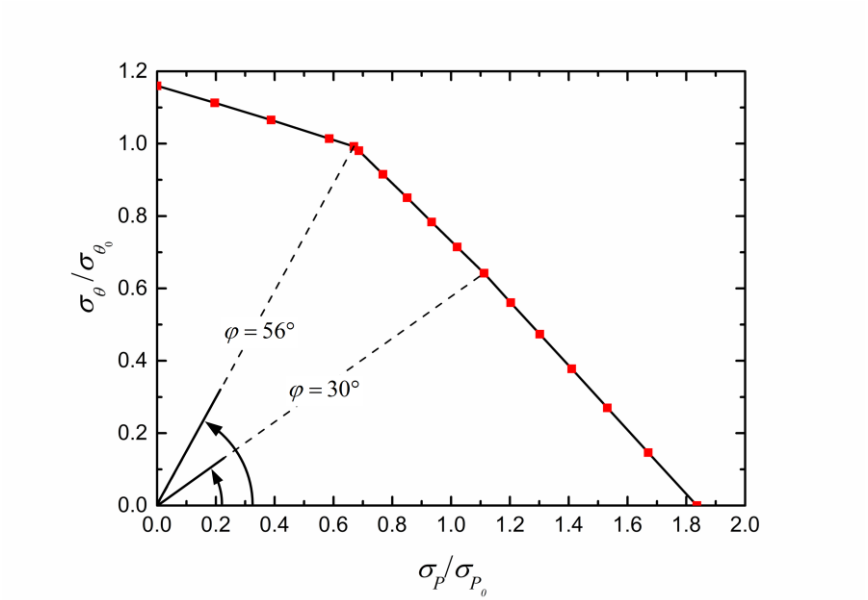

689

690 **Fig. 25.** Shakedown domain for the thick vessel with nozzles.

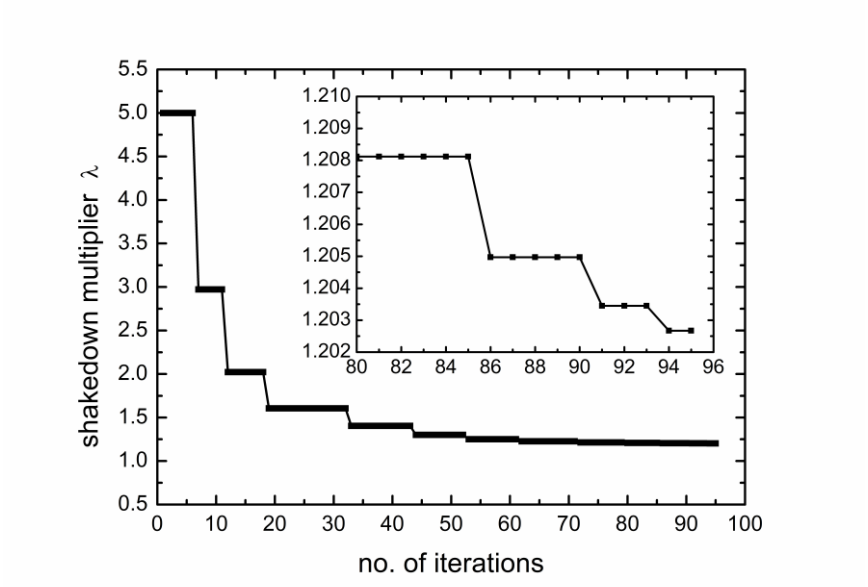

691

692 **Fig. 26.** Iterative convergence process of the shakedown multiplier for the load combination

693 $$\sigma_\theta/\sigma_{\theta_0} = \sigma_{\mathrm{P}}/\sigma_{\mathrm{P}_0}\ .$$

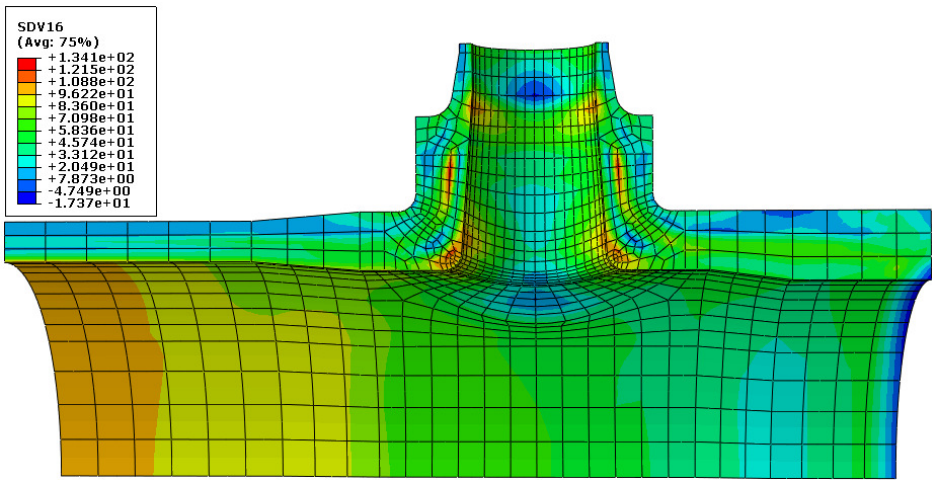

Fig. 27. Von Mises residual stress field of the thick vessel with nozzles for the load combination $\sigma_\theta/\sigma_{\theta_0}=\sigma_{\mathrm{P}}/\sigma_{\mathrm{P}_0}$.

6 Conclusions

A novel numerical procedure based on the Stress Compensation Method (SCM) for shakedown analysis of engineering structures under multiple variable mechanical and thermal loads is proposed. The presented methodology has been implemented into ABAQUS platform to investigate the Bree problem and the shakedown domains of a square plate with a central circular hole under various three-dimensional loading domains, and to solve the practical shakedown problems of a thick vessel with nozzles. The following conclusions can be made:

1. With no need to perform mathematical programming, the proposed numerical method for shakedown analysis is a two-level iterative procedure, where just a series of linear finite element analyses with same global stiffness matrix are performed and the global stiffness matrix is decomposed only once. The novel strategy for constructing the residual stress field makes the global equilibrium equations solved only at the end of a load cycle instead of at every load vertex. Therefore, the computational cost of shakedown analysis has little relationship with the number of vertices of loading domain.
2. Three types of the Bree problem verify the effectiveness of the SCM. Three shakedown domains of the square plate with a circular hole under three loading cases are obtained and different mechanisms involving alternating plasticity and ratcheting to determine the shakedown boundaries are revealed. For the thick vessel with nozzles under the given

loading cases, the shakedown boundaries are dominated by the alternating plasticity mechanism.

3. The iterative process of shakedown analysis by the SCM presents good convergence. The proposed numerical procedure turns out to be of good numerical stability, high accuracy and efficiency, and is well suited for shakedown analysis of large-scale engineering structures under multi-dimensional loading domain.
4. Although the present applications are limited to the elastic-perfectly plastic material with von Mises yield surface and the material properties are independent of the temperature, the extensions to consideration of the hardening material and the temperature-dependent yield stress are in progress, and the results will be reported in forthcoming works.

Acknowledgments

The authors would like to acknowledge the support of the National Science Foundation for Distinguished Young Scholars of China (Grant No.11325211), the National Natural Science Foundation of China (Grant No.11672147) and the Project of International Cooperation and Exchange NSFC (Grant No. 11511130057) during this work.

References

[1] Borkowski A, Kleiber M. On a numerical approach to shakedown analysis of structures. Comput Method Appl M 1980;22:101-119.

[2] Kleiber M, König JA. Incremental shakedown analysis in the case of thermal effects. Int J Numer Meth Eng 1984;20:1567-1573.

[3] Melan E. Zur Plastizität des räumlichen Kontinuums. Ingenieur-Archiv 1938;9:116-126.

[4] Koiter WT, General theorems for elastic-plastic solids, in: Sneddon, JN, Hill, R (Eds.) Progress in Solid Mechanics, North-Holland: Amsterdam, 1960, pp. 167-221.

[5] König JA, Shakedown of elastic-plastic structures, Elsevier, Amsterdam, 1987.

[6] Maier G. Shakedown theory in perfect elastoplasticity with associated and nonassociated flow laws: A finite element linear programing approach. Meccanica 1969;4:250-260.

[7] Li HX. Kinematic shakedown analysis under a general yield condition with non-associated plastic flow. Int J Mech Sci 2010;52:1-12.

[8] Weichert D, Hachemi A. Influence of geometrical nonlinearities on the shakedown of damaged structures. Int J Plasticity 1998;14:891-907.

[9] Polizzotto C, Borino G, Caddemi S, Fuschi P. Theorems of restricted dynamic shakedown. Int J Mech Sci 1993;35:787-801.

[10] Maier G, Novati G. Dynamic Shakedown and Bounding Theory for a Class of Nonlinear

748 Hardening Discrete Structural Models. Int J Plasticity 1990;6:551-572.
749 [11] Hachemi A, Weichert D. Application of shakedown theory to damaging inelastic material under
750 mechanical and thermal loads. Int J Mech Sci 1997;39:1067-1076.
751 [12] Stein E, Huang Y. An analytical method for shakedown problems with linear kinematic hardening
752 materials. Int J Solids Struct 1994;31:2433-2444.
753 [13] Nayebi A, El Abdi R. Shakedown analysis of beams using nonlinear kinematic hardening
754 materials coupled with continuum damage mechanics. Int J Mech Sci 2008;50:1247-1254.
755 [14] Leu SY, Li JS. Shakedown analysis of truss structures with nonlinear kinematic hardening. Int J
756 Mech Sci 2015;103:172-180.
757 [15] Le CV, Tran TD, Pham DC. Rotating plasticity and nonshakedown collapse modes for elastic–
758 plastic bodies under cyclic loads. Int J Mech Sci 2016;111–112:55-64.
759 [16] Simon JW. Direct evaluation of the limit states of engineering structures exhibiting limited,
760 nonlinear kinematical hardening. Int J Plasticity 2013;42:141-167.
761 [17] Belytschko T. Plane stress shakedown analysis by finite elements. Int J Mech Sci
762 1972;14:619-625.
763 [18] Janas M, Pycko S, Zwoliński J. A min-max procedure for the shakedown analysis of skeletal
764 structures. Int J Mech Sci 1995;37:629-643.
765 [19] Xue MD, Wang XF, Williams FW, Xu BY. Lower-bound shakedown analysis of axisymmetric
766 structures subjected to variable mechanical and thermal loads. Int J Mech Sci 1997;39:965-976.
767 [20] Zouain N, Borges L, Silveira JL. An algorithm for shakedown analysis with nonlinear yield
768 functions. Comput Method Appl M 2002;191:2463-2481.
769 [21] Khoi VUD, Yan A-M, Hung N-D. A dual form for discretized kinematic formulation in
770 shakedown analysis. Int J Solids Struct 2004;41:267-277.
771 [22] Vu DK, Yan AM, Nguyen-Dang H. A primal–dual algorithm for shakedown analysis of structures.
772 Comput Method Appl M 2004;193:4663-4674.
773 [23] Makrodimopoulos A, Martin CM. Lower bound limit analysis of cohesive-frictional materials
774 using second-order cone programming. Int J Numer Meth Eng 2006;66:604-634.
775 [24] Bisbos CD, Makrodimopoulos A, Pardalos PM. Second-order cone programming approaches to
776 static shakedown analysis in steel plasticity. Optim Method Softw 2005;20:25-52.
777 [25] Krabbenhoft K, Lyamin AV, Sloan SW. Shakedown of a cohesive-frictional half-space subjected
778 to rolling and sliding contact. Int J Solids Struct 2007;44:3998-4008.
779 [26] Nguyen AD, Hachemi A, Weichert D. Application of the interior-point method to shakedown
780 analysis of pavements. Int J Numer Meth Eng 2008;75:414-439.
781 [27] Garcea G, Leonetti L. A unified mathematical programming formulation of strain driven and
782 interior point algorithms for shakedown and limit analysis. Int J Numer Meth Eng
783 2011;88:1085-1111.
784 [28] Simon JW, Weichert D. Numerical lower bound shakedown analysis of engineering structures.
785 Comput Method Appl M 2011;200:2828-2839.
786 [29] Simon JW, Weichert D. Shakedown analysis with multidimensional loading spaces. Comput
787 Mech 2012;49:477-485.
788 [30] Liu YH, Zhang XF, Cen ZZ. Lower bound shakedown analysis by the symmetric Galerkin
789 boundary element method. Int J Plasticity 2005;21:21-42.
790 [31] Le CV, Nguyen-Xuan H, Askes H, Bordas SPA, Rabczuk T, Nguyen-Vinh H. A cell-based
791 smoothed finite element method for kinematic limit analysis. Int J Numer Meth Eng

2010;83:1651-1674.
[32] Tran TN, Liu GR, Nguyen-Xuan H, Nguyen-Thoi T. An edge-based smoothed finite element method for primal–dual shakedown analysis of structures. Int J Numer Meth Eng 2010;82:917-938.
[33] Nguyen-Xuan H, Rabczuk T, Nguyen-Thoi T, Tran TN, Nguyen-Thanh N. Computation of limit and shakedown loads using a node-based smoothed finite element method. Int J Numer Meth Eng 2012;90:287-310.
[34] Chen S, Liu Y, Cen Z. Lower bound shakedown analysis by using the element free Galerkin method and non-linear programming. Comput Method Appl M 2008;197:3911-3921.
[35] Do HV, Nguyen-Xuan H. Limit and shakedown isogeometric analysis of structures based on Bézier extraction. European Journal of Mechanics - A/Solids 2017;63:149-164.
[36] Ponter ARS, Carter KF. Shakedown state simulation techniques based on linear elastic solutions. Comput Method Appl M 1997;140:259-279.
[37] Ponter ARS, Engelhardt M. Shakedown limits for a general yield condition: implementation and application for a Von Mises yield condition. Eur J Mech a-Solid 2000;19:423-445.
[38] Chen HF, Ponter ARS. Shakedown and limit analyses for 3-D structures using the linear matching method. International Journal of Pressure Vessels and Piping 2001;78:443-451.
[39] Chen HF, Ponter ARS. A method for the evaluation of a ratchet limit and the amplitude of plastic strain for bodies subjected to cyclic loading. Eur J Mech a-Solid 2001;20:555-571.
[40] Lytwyn M, Chen HF, Ponter ARS. A generalised method for ratchet analysis of structures undergoing arbitrary thermo-mechanical load histories. Int J Numer Meth Eng 2015;104:104-124.
[41] Spiliopoulos KV, Panagiotou KD. A Residual Stress Decomposition based Method for the Shakedown analysis of structures. Comput Method Appl M 2014;276:410-430.
[42] Tin-Loi F, Ngo NS. Performance of a p-adaptive finite element method for shakedown analysis. Int J Mech Sci 2007;49:1166-1178.
[43] Groβ-Weege J. On the numerical assessment of the safety factor of elastic-plastic structures under variable loading. Int J Mech Sci 1997;39:417-433.
[44] Chinh PD. Evaluation of shakedown loads for plates. Int J Mech Sci 1997;39:1415-1422.
[45] Barbera D, Chen H, Liu Y, Xuan F. Recent Developments of the Linear Matching Method Framework for Structural Integrity Assessment. Journal of Pressure Vessel Technology 2017;139:051101-051109.
[46] Spiliopoulos KV, Panagiotou KD. A numerical procedure for the shakedown analysis of structures under cyclic thermomechanical loading. Arch Appl Mech 2015;85:1499-1511.
[47] ABAQUS. Dassault Systems, Version 6.14, 2014.
[48] Bree J. Elastic-plastic behaviour of thin tubes subjected to internal pressure and intermittent high-heat fluxes with application to fast-nuclear-reactor fuel elements. Journal of strain analysis 1967;2:226-238.
[49] Bradford RAW. The Bree problem with primary load cycling in-phase with the secondary load. International Journal of Pressure Vessels and Piping 2012;99–100:44-50.
[50] Garcea G, Armentano G, Petrolo S, Casciaro R. Finite element shakedown analysis of two-dimensional structures. Int J Numer Meth Eng 2005;63:1174-1202.